Istraživanja i projektovanja za privredu
ISSN 1451-4117
DOI:10.5937/jaes0-40698
www.engineeringscience.rs

iipp publishing

Journal of Applied Engineering Science
Vol. 21, No. 2, 2023
Original Scientific Paper
Paper number: 21(2023)2, 1094, 501-531

FAST PATROL BOAT HULL DESIGN CONCEPTS ON HYDRODYNAMIC PERFORMANCES AND SURVIVABILITY EVALUATION

Angga Sifta Pratama[1], Aditya Rio Prabowo[1,*], Tuswan Tuswan[2,*], Ristiyanto Adiputra[3], Nurul Muhayat[1], Bo Cao[4], Syamsul Hadi[1], Indri Yaningsih[1]

[1] *Department of Mechanical Engineering, Universitas Sebelas Maret, Surakarta 57126, Indonesia*
[2] *Department of Naval Architecture, Universitas Diponegoro, Semarang 50275, Indonesia*
[3] *Research Center for Hydrodynamics Technology, National Research and Innovation Agency (BRIN), Surabaya 60112, Indonesia*
[4] *China Shipbuilding Industry Corporation Economic Research Center, Beijing 100097, China*
** aditya@ft.uns.ac.id (A.R.P.); tuswan@lecturer.undip.ac.id (T.T.)*

A fast patrol boat is one of the ships intended to defend a region and rescue and search in the accident event so that the ship must have a high level of security and survivability performances. This study uses 9 design variations with various main dimensions and hull lengths to determine the effect of the different main dimensions on the hydrodynamic performances. Each criterion was affected to obtain results in hull design, durability, stability, seakeeping, floodable length, and motion sickness incidence (MSI). Simulations are carried out to determine the resistance, stability, ship response when exposed to external forces, passenger comfort, and ship safety level when a leak occurs. Resistance simulation uses a Froude number between 0 to 2.217. Stability simulation analyzes max GZ and angle of maximum GZ on seakeeping, deck wetness, and MSI simulations using 90°, 135°, and 180° wave incidence angles. The addition of bulkheads is carried out to determine the ship's response when it experiences a leak and prevents the ship's sinking when puddles enter the ship with five bulkheads per hull and three variations in distance. Design and simulation of various criteria using Maxsurf software. In the floodable length simulation, the hull added a bulkhead to determine the effect of leakage from several hull designs and watertight bulkhead spacing variations. Design 7 has the best average result compared to other designs from the simulation recapitulation results. It has a small resistance value, a large stability angle, a stable ship response when subjected to external forces, seasickness levels, and a small deck language. From the floodable length graph, it has a high flood limit that makes the ship survive and be safer than other designs. Design 7 refers to the ship Grandweld Shipyard Delivers 21M Discovery Class Vessel Fujairah Pilot.

Keywords: fast patrol boat, floodable length, bulkhead, survivability

1 INTRODUCTION

Indonesia is a large country with a larger water area than land area. As a large country, Indonesia needs to have a strong sea defensive system. The strategic sea route is one of the advantages that can be used to support the economy, the many routes that can be passed make it easier to trade both exports and imports [1]. Abundant natural resources can be used by the community to support life. However, its strategic location and abundant resources make crime rife in Indonesian waters [2]. Illegal fishing, robbery, shifting territorial boundaries are problems that must be watched out for and overcome [3]. The rise of problems and crimes in water areas is caused by several factors, including a weak legal system and lack of patrol supervision [2–4]. The development of maritime defense will give birth to a defense vision that makes the military fleet stronger. Strengthening and adding to the fleet in Indonesia is one way to anticipate these problems. Weak weapon systems and ship performance will make the sea defenses easily defeated by the enemy. So we need a reliable defense system with a complete and more sophisticated weapon system [5]. In addition to weapons systems, a ship must have reliable capabilities in carrying out operations and patrols.

The fast patrol boat is a ship with high mobility in carrying out a mission. Fast patrol boats are important in guarding an area because they have good mobility and capabilities in various conditions [2]. This ship can operate to guard a wide area, perform various naval missions and government duties, and carry out rescues [6]. Fast patrol boats are designed to have speed, maneuverability, and endurance in various water conditions [7]. The monohull type is often used because the monohull is a fast boat hull, so it supports operations [8]. V-shaped hull is a type that is suitable to be applied to fast patrol boats because it has good maneuverability, high speed, and little friction or small resistance when the ship is sailing [9]. The selection of V-shaped hull also requires analysis and calculation to get the most efficient value to be applied to Indonesian waters.

When designing a ship, the fundamental part that needs to be considered is the stability and buoyancy of the boat to ensure safety when the ship sails [10]. IMO (International Maritime Organization) integrates criteria regarding property correction lever curves for ship stability standards. Another critical factor in designing a ship must also pay attention to the friction and resistance of the vessel to water fluids. High-speed ships such as fast patrol boats need to pay attention to two conditions, namely fuel consumption and passenger comfort [11]. In order to support the ship's

performance, seakeeping analysis is also needed to analyze the ship's motion from the influence of external wave forces. Seakeeping criteria will affect several aspects, such as decreased speed, operational systems, and passenger comfort [12]. Fast patrol boats with high speed will also affect the level of drunkenness of the crew later. Passenger comfort can be determined by analyzing the MSI (Motion Sickness Incidence) calculation. The effect of high sea waves can make passengers drunk and also wet the ship's deck. Deck wetness will be a double burden for the ship, which results in a decrease in the performance and effectiveness of a ship [13]. These factors will be considered in designing a fast patrol boat to get an effective model.

Ship accidents are things that can happen to ships while sailing even though they have been calculated and analyzed in the design. Accidents can occur due to collisions, capsizing due to water entering the ship, and casualties during the war [14]. In addition to variations in hull design, variations in bulkhead placement are also needed to prevent the ship from leaking. The addition of this bulkhead prevents puddles of water from filling the ship's room and crossing the flood boundary line so that the ship can survive the sinking [15]. This study analyzes the factors that affect the ship's performance, especially the design and simulation process. The fast patrol boat hull design is made into several variations and integrated with bulked variations to get optimal fast patrol boat performance.

2 LITERATURE REVIEW

2.1 General Definition of a Fast Patrol Boat

Fast patrol boats are designed to have speed, maneuverability, and a sturdy structure in sailing on the high seas [7]. High performance and various criteria, of course, must be owned by a fast patrol boat to support the mission. Fast patrol boats have the main capabilities, namely high speed and agility. Besides sailing, they are also equipped with weapons to increase security in the waters area [16]. Fast patrol boats usually operate at sea borders to protect against marine crimes, smuggling, and piracy [17]. Coastal protection and corruption need to be overcome using fast patrol boats that are superior to enemy ships. These ships are usually armed with torpedoes, missiles, and small-caliber weapons [18]. The construction and materials used must also be sturdy and strong to withstand a collision or shot when carrying out a mission [19]. Careful calculations in the design are needed because fast patrol boats sail at high speeds and require good stability when driving and maneuvering. In addition to good performance, it is also necessary to consider aspects to anticipate when an accident occurs and the comfort of the crew on board. Rules for patrol vessels or Military Vessels are found in several registers such as Registro Italiano Navale (RINA), Lloyd's Register (LR), and Det Norske Veritas (DNV). Several rules are presented in Table 1, and the military strength of major countries from rank one to nine and Indonesia is shown in Fig. 1 to Fig. 10.

Table 1. Comparison of ship rules reference for patrol vessels or military vessels

Class society	Code	Reference	Title	Characteristic
Lloyd's Register	Volume 1, Part 4, Chapter 1 Section 2	Lloyd's Register – classification, training and advisory services https://www.lr.org/en/	Vulnerability	2.2.1 The resistance of a vessel to loadings from military threats can be described by the term vulnerability which is the probability that once hit by a specified threat a vessel will lose capability
	Volume 1, Part 5, Chapter 3 Section 1		Local Design Load	1.3.2 Froude Number F n. The Froude number is a nondimensional parameter which is the primary constituent part of the wave making resistance and which dictates the maximum displacement speed.
	Volume 2, Part 1, Chapter 3 Section 4		Requirements for Design, Construction, Installation and Sea Trials of Engineering Systems	4.10.4 The techniques that may be employed for control of underwater signature are: (d) The hull form should be fair and smooth to minimise resistance and flow noise.
	Volume 1, Part 3, Chapter 1 Section 5		General	5.11.1 The minimum extent of watertight subdivision (internal), and integrity (internal and external), is to be in accordance with the specified subdivision and stability standard(s).

Class society	Code	Reference	Title	Characteristic
	Volume 1, Part 3, Chapter 2 Section 1		Ship Design	1.3.3 Intact stability calculations to satisfy the applicable criteria may be based on the buoyancy of the main hull, together with any superstructures that have watertight and weathertight boundaries.
	Volume 1, Part 3, Chapter 2 Section 1		Ship Design	1.3.7 Typically there are two approaches to defining the limits of watertight and weathertight integrity: (b) The other is based on watertight integrity up to a damaged stability draft and heel envelope, the latter is commonly used by Navies.
	Volume 1, Part 3, Chapter 2 Section 4		Ship Design	4.2.1 In general, the number and disposition of bulkheads are to be arranged to suit the requirements for subdivision, floodability and damage stability, and are to be in accordance with the specified subdivision and stability standard(s).
	Volume 3, Part 1, Chapter 5 Section 7		Replenishment at Sea (RAS) Systems	7.3.1 The seakeeping and manoeuvrability characteristics of the ship are to be assessed and the requirements of the class notation LMA in Vol 3, Pt 1, Ch 4 Manoeuvring Assessment are to be complied with as applicable.
DNV AS Rules for Classification High speed and light craft	Part 3, Chapter 1 Section 3	Rules and standards – DNV https://www.dnv.com/rules-standards/index.html	General	1.1.2 New design concepts may require tank tests, theoretical studies, or full scale measurements to establish seakeeping properties and design loads.
	Part 3, Chapter 1 Section 2		Subdivision and arrangement	1.2.1 At least the following transverse watertight bulkheads shall be fitted: — a collision bulkhead — a bulkhead at each end of the machinery space(s).
	Part 3, Chapter 1 Section 2		Subdivision and arrangement	1.3.1 The distance xC from the forward perpendicular to the collision bulkhead shall be taken between the following limits: xC (minimum) = 0.05 L (m) xC (maximum) = 3.0 + 0.05 L (m) An increase of the maximum distance given above may be acceptable upon consideration in each case, provided a floatability and stability calculation shows that, with the craft fully loaded to summer draught on even keel, flooding of the space forward of the collision bulkhead will not result in any other compartments being flooded, nor in an unacceptable loss of stability.
	Part 5, Chapter 5 Section 2		Watertight Integrity and Buoyancy	1.5.1 The stability requirements for assignment of main class shall be complied with. Guidance note: For information and guidance to the master, curves should be presented showing wind speeds, for which the IMO weather criterion

Class society	Code	Reference	Title	Characteristic
				is in compliance with, for the craft's draught range.
RINA - Rules for The Classification of Fast Patrol Vessels	Part B, Chapter 3, Section 2	Rules for naval ships classification - RINA.org https://www.rina.org/en/rules-for-naval-ships	Design criteria	2.1.1 General The standard of stability to be achieved by a new vessel should be dependent on the maximum number of persons permitted to be carried and the intended area of operation (navigation notation).
	Part B, Chapter 3, Section 2		Design criteria	2.1.2 GZ curve area. The area under the righting lever curve (GZ curve) is to be not less than 0,055 m. rad up to θ = 30° angle of heel and not less than 0,09 m. rad up to θ = 40° or the angle of down flooding θf if this angle is less than 40°. Additionally, the area under the righting lever curve (GZ curve) between the angles of heel of 30° and 40° or between 30°and θf, if this angle is less than 40°, is to be not less than 0,03 m. rad.
	Part B, Chapter 3, Section 2		Design criteria	2.1.3 Minimum righting lever. The righting lever GZ is to be at least 0,20 m at an angle of heel equal to or greater than 30°
	Part B, Chapter 3, Section 2		Design criteria	2.1.4 Angle of maximum righting lever. The maximum righting arm is to occur at an angle of heel preferably exceeding 30° but not less than 25°. When the righting lever curve has a shape with two maximums, the first is to be located at a heel angle not less than 25°. In cases of vessels with a particular design and subject to the prior agreement of the flag Administration, RINA may accept an angle of heel θmax less than 25° but in no case less than 15°, provided that the area "A" below the righting lever curve is not less than the value obtained, in m.rad, from the following formula: A = 0,055 + 0,002 (30° - θmax) where θmax is the angle of heel in degrees at which the righting lever curve reaches its maximum.
	Part B, Chapter 3, Section 3		Buoyancy and stability in the displacement mode following damage	2.1.1 The full load vessel is to present a residual positive metacentric height and limit line not submerged at the final phase of overflowing with any flooded compartment.
	Part B, Chapter 3, Section 3		Buoyancy and stability in the displacement mode following damage	2.2.3 Buoyancy and stability in damage Following any of the postulated damages detailed in [2.2.1] and [2.2.2] the vessel, in still water, shall have sufficient buoyancy and positive stability to ensure simultaneously that:

Class society	Code	Reference	Title	Characteristic
				1. after flooding has ceased and a state of equilibrium has been reached, the final waterline is below the level of any opening through which further flooding could take place by at least 50% of the significant wave height corresponding to the worst intended conditions. Downflooding openings shall include doors and hatches which are used for damage control or evacuation procedures, but may exclude those which are closed by means of weathertight doors and hatch cover and not used for damage control or evacuation procedures.
	Part B, Chapter 2, Section 1		Number and arrangement of transverse watertight bulkheads	1.1.1 General. All vessels, in addition to complying with the requirements of [1.1.2], are to present at least the following transverse watertight bulkheads: • one collision bulkhead, • one after peak bulkhead, • two bulkheads forming the boundaries of the machinery space in vessels with machinery amidships, and a bulkhead forward of the machinery space in vessels with machinery aft. In the case of vessels with an electrical propulsion plant, both the generator room and the engine room are to be enclosed by watertight bulkheads.

Table 1 is a comparison of ship rules for patrol vessels. The rules for the fast patrol boat are used as a reference in the study's hull fast patrol boat design. References and characteristics taken are the part that will relate to the research conducted. Characteristics used as a reference, such as parameters in the simulation and testing to be carried out.

Fig. 1. Military strength of United States

United States will occupy the first position in military strength in the waters area by 2022. United States became the strongest country, with 92 destroyers, 68 submarines, and 11 aircraft carriers. United States has several fast patrol

boats and various classes such as Cyclone-class, Tacoma-class, and others. In addition, Mine Warfare type defense equipment, Corvettes, and Helicopter Carries increase the strength of the United States military.

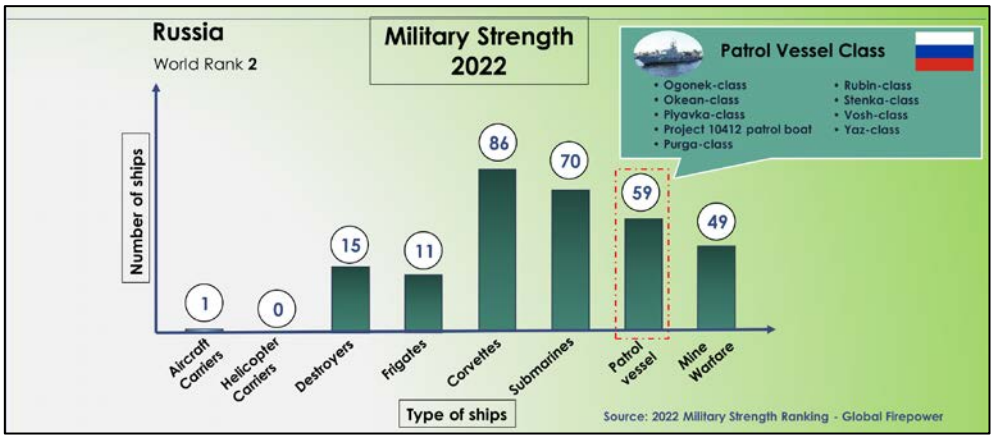

Fig. 2. Military strength of Russia

Russia occupies the second position after the United States in military strength in the waters area in 2022. Russia's military strength is supported by various defense equipments, such as 86 Corvettes, 70 Submarines, and 59 Patrol Vessels. Russian patrol vessels are divided into several classes, such as Ogonek-class, Yaz-class, and others. Russia's military strength is also supported by Aircraft Carriers, Destroyers, Frigates, and Mine Warfare.

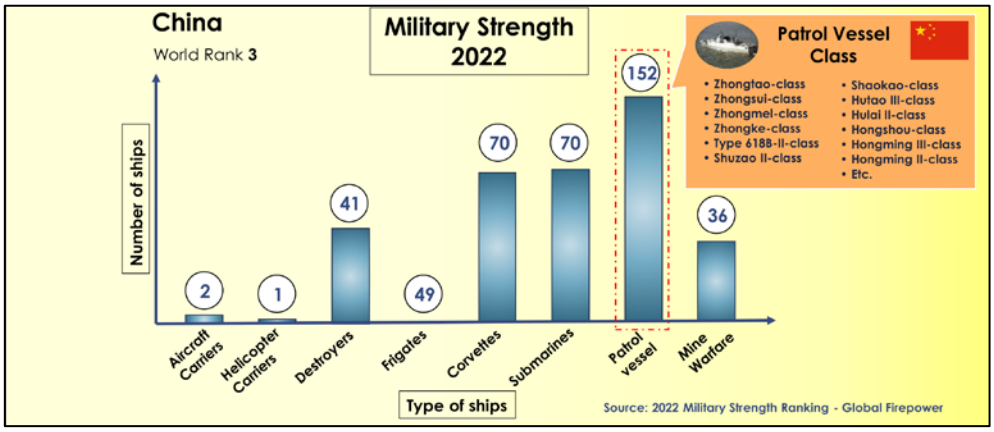

Fig. 3. Military strength of China

China is the country with the third strongest military strength in 2022. China has 152 Patrol Vessels, 70 Corvettes, and 70 Submarines. In addition, China is also strengthened by the presence of Aircraft Carriers, Helicopter Carriers, Destroyers, Frigates, and Mine Warfare. Patrol vessels in China's military strength are divided into several classes: Zhongtao-class, Zhongsui-class, and others.

Fig. 4. Military strength of India

Military Strength in the waters area in 2022 ranks fourth in the country India. India is reinforced with 128 Patrol Vessels, 17 Submarines, and 22 Corvettes. Patrol vessels in Military India are divided into several classes, including Bangaram-class, Ajay-class, and others. In addition, there are also ships with the type of Aircraft Carriers, Destroyers, and Frigates that make India stronger.

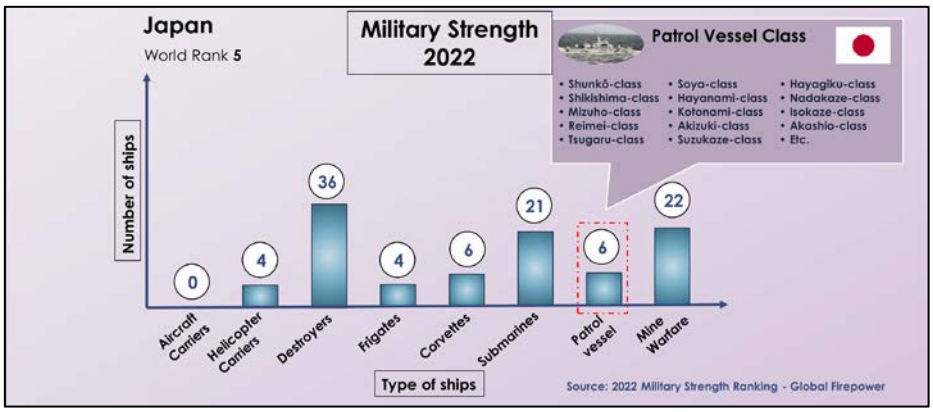

Fig. 5. Military strength of Japan

Japan ranks fifth in Military Strength in the territorial waters in 2022. Japan has 36 destroyers, 21 Submarines, and 22 Mine Warfare. Japan also has several Patrol Vessels with various classes, including Mizuno-class, Shikishima-class, and others. Japan is also strengthened by Helicopter Carriers, Frigates, and Corvettes.

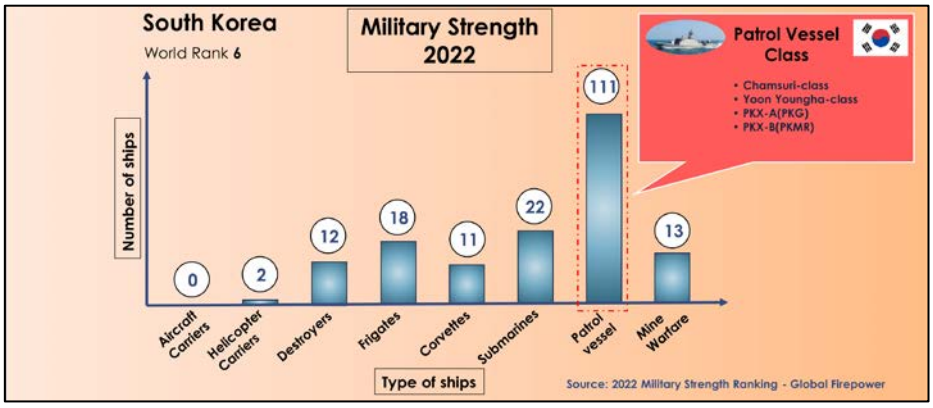

Fig. 6. Military strength of South Korea

South Korea is the country with the sixth strongest Military Strength in 2022. There are 111 patrol vessels in South Korea with various classes, including Chamsuri-class, Yoon Youngha-class, and others. In addition to a large number of patrol vessels, South Korea is also reinforced with Helicopter Carriers, Destroyers, Frigates, Corvettes, Submarines, and Mine Warfare.

Fig. 7. Military strength of France

Military strength 2022 in the waters area to which there is a country France. France has 17 Mine Warfare, 15 Patrol Vessels, and 10 Submarines. The patrol vessel is divided into several classes: Flamant-class, Confiance-class, and others. France is also strengthened by Aircraft Carriers, Helicopter Carriers, Destroyers, and Frigates.

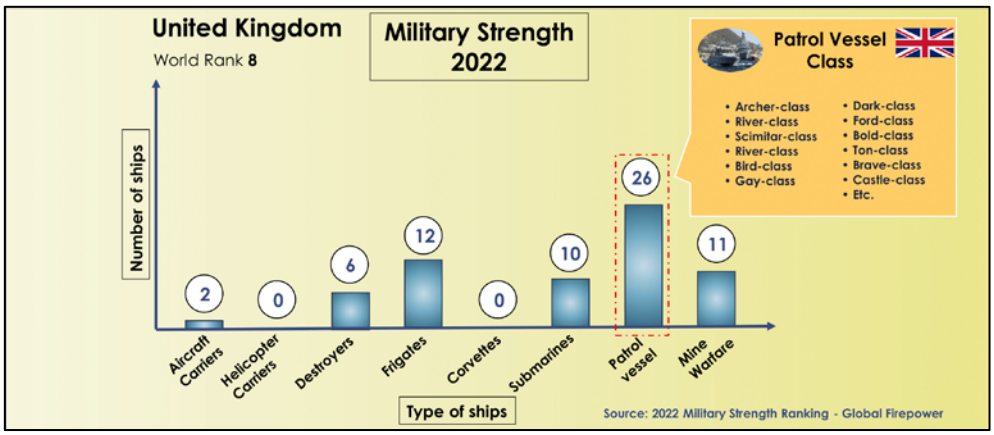

Fig. 8. Military strength of United Kingdom

The United Kingdom ranks eighth in Military Strength in 2022. The United Kingdom has 26 Patrol Vessels, 12 Frigates, and 10 Submarines. Patrol vessels in the United Kingdom are divided into Archer-class, River-class, and others. In addition, the United Kingdom has defense equipment in the form of Aircraft Carriers, Destroyers, and Mine Warfare.

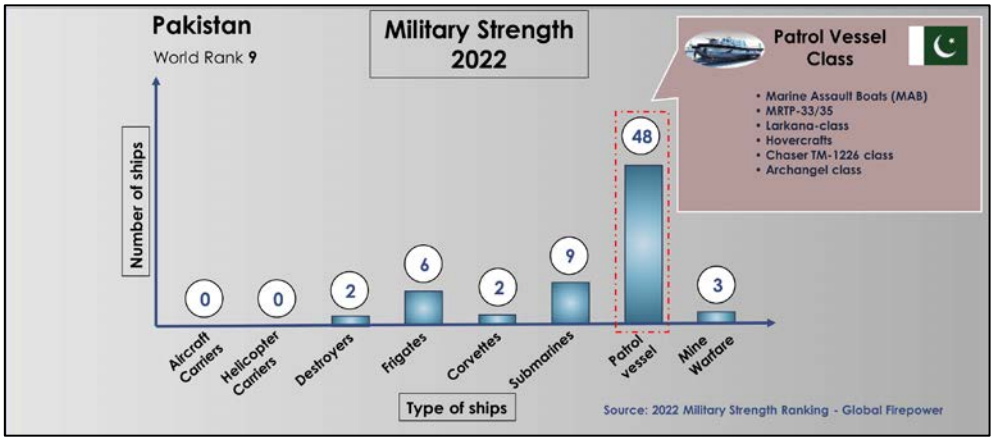

Fig. 9. Military strength of Pakistan

The ninth order in Military Strength 2022 is Pakistan, with the most Patrol Vessel defense equipment. Pakistan has 48 Patrol Vessels, 9 submarines, and 6 Frigates. Patrol vessels in Pakistan are divided into several classes, namely Larkana-class, Archangel-class, and other classes. In addition, Pakistan is also strengthened with Destroyers, Corvettes, and Mine Warfare.

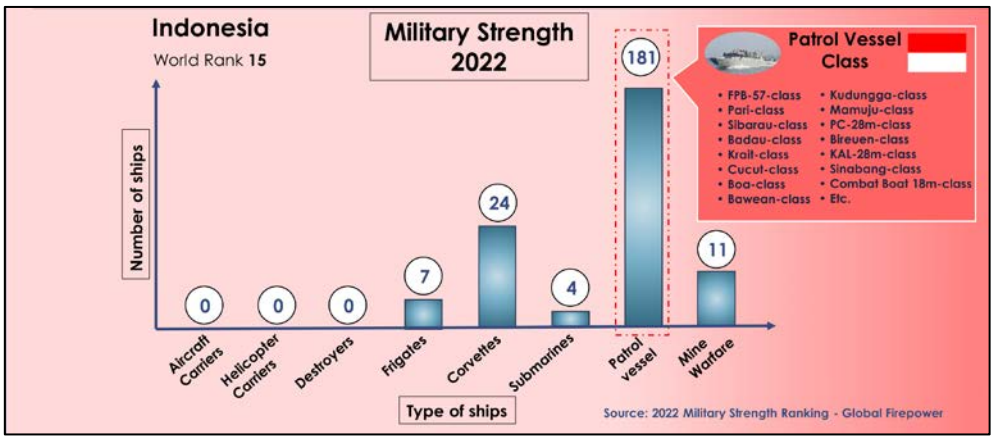

Fig. 10. Military strength of Indonesia

Indonesia is the fifteenth strongest country in Military Strength 2022. Indonesia has the most autism with the Patrol Vessel type. There are 181 Indonesian Patrol Vessels with various classes, including Pari-class, Sibarau-class, and others. Apart from Patrol Vessels, Indonesia was also reinforced with 7 Frigates, 24 Corvettes, 4 Submarines, and 11 Mine Warfare.

2.2 Hull Resistance Analysis

Ship resistance is the reaction between the hull of the ship and the fluid due to the ship's movement through the fluid [17]. A ship has resistance because a force is opposite the ship's direction [20]. Resistance will always have an effect when the ship sails, so the shape of the hull will affect the level of resistance of a ship. In addition to the shape of the hull, the resistance value can also be affected by the ship's speed and the ship's displacement [21]. So, the boat's design is designed to have a minimum resistance value so that the ship operates optimally. The total resistance value received by the ship consists of Frictional resistance, Viscous resistance, and Wave resistance [22].

Frictional resistance is affected by fluid viscosity, vessel speed, and wet area [20]. The general formula based on the 1975 International Towing Tank Conference (ITTC) is shown in Eq. 1 and 2.

$$C_f = \frac{0.075}{(\log R_n - 2)^2} \tag{1}$$

$$C_f = \frac{R_f}{\frac{1}{2}\rho S V^2} \tag{2}$$

Viscous resistance is caused by the viscosity of the fluid and the asymmetric flow around the hull, causing the boundary layer and density to elongate [23]. Viscous resistance can be calculated by the correlation line ITTC-1957 and the hull are obtain for experiment form factor (1+k), shown in the following Eq. 3 [24].

$$C_v = (1+k)C_f \tag{3}$$

Wave resistance is mainly generated due to the hull's shape at the closest part of the surface [24]. The wave resistance can be neglected at high speeds because its value is relatively small. The ship will be more affected by high-speed friction on the wet surface area. [20]. The wave resistance value can be found by the following Eq. 4.

$$R_w = c_1 c_2 c_3 \nabla \rho g \exp\left\{m_1 F_r^g + m_4 \cos(\lambda F_r^{-2})\right\} \tag{4}$$

2.2.1 Froude Number and Reynold Number

In ITTC standard, the Reynolds number will affect the viscosity resistance, and the Froude number will affect the wave resistance of the ship [23]. The friction between the hull and the fluid being passed is influenced by the Froude number and Reynolds number, where these numbers determine the value of friction drag and wave drag [25]. Reynolds number is a parameter used to identify the type of fluid [20]. The Reynolds number is affected by the fluid viscosity and the inertial force, which is shown in the following Eq. 5 [26].

$$R_n = \frac{V_s L_s}{\nu} \tag{5}$$

The value of the ship's Froude number adjusts to the length of the ship, the point submerged in water, and based on the depth of immersion [27]. Froude number is a dimensionless number to determine the model criteria in hydrodynamics [20]. The Froude number value is also a comparison between the ship's speed and the ship displacement [28]. The following equation can determine the Froude number value using Eq. 6.

$$F_n = \frac{V_s}{\sqrt{g L_s}} \tag{6}$$

2.2.2 Savitsky Method

There are several methods that can be used to calculate the resistance value, one of which is the Savitsky method [29]. The Savitsky method is a numerical method for calculating the value of ship resistance. The Savitsky method develops an equation to determine the planning hull using certain geometric parameters that calculate the wetted area, lift, drag, the center of pressure, and stability limits [30]. The power and fuel used will adjust the driving force in overcoming the resistance when the ship moves so that an increase in the ship's hull characteristics is needed to get a smaller resistance value [31]. The value of frictional resistance can be found in the Savitsky method in the following Eq. 7.

$$D_f = \frac{C_f \rho v_1^2 \left(\lambda b^2\right)}{2\cos\beta} \tag{7}$$

The friction value can be used to find the total drag value with an Eq. 8.

$$D = \Delta \tan \tau + \frac{D_f}{\cos \tau} \tag{8}$$

2.3 Large Angle Stability

Stability on the ship is the essential part for the ship to return to its equilibrium position when under the influence of external forces that disturb the balance of the ship [32]. Stability is divided into two based on the condition of a ship [10], namely: intact stability is the ship's ability to maintain ship stability against external moments without affecting ship operations. Damage stability is the ship's ability to maintain conditions so that it does not overturn when damage occurs. IMO (International Maritime Organization) defines stability as one of the safety aspects when carrying out designs [33]. Stability is the nature or tendency of the ship to return to the equilibrium position due to the influence of external forces, and stability also depends on the hull form factor and load distribution [34].

2.3.1 Righting Lever Curve

The righting lever curve (GZ) is one factor in measuring the ship stability level. GZ is a factor to describe the ship's ability to withstand heeling moments against external forces [35]. Considering IMO standardization, the maximum value of the righting lever angle should not be less than 25° using Eq. 9.

$$\frac{dGZ}{d\phi}\left(\phi \geq 25°\right) = 0 \tag{9}$$

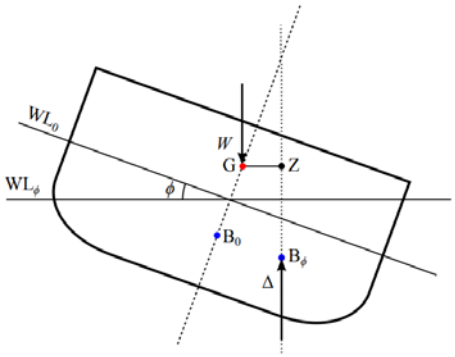

Fig. 11. Definition of the righting lever GZ

In Fig. 11, the center of initial buoyancy (B_0), the center of gravity shifts (B_ϕ) when the ship is exposed to an external force [35]. The liquid load will shift the center of gravity, and the buoyant force has the same value as the ship's weight (*W*) but the direction of the force is opposite [35].

2.3.2 IMO A.749(18) Code on Intact Stability

Criteria for the development of national regulations and community classification with first-generation stability standards are listed in IMO Res A.749 (18) [36]. In this study, in analyzing the stability of the ship design using the IMO (International Maritime Organization) standard reference A.749(18) Ch3 - Design criteria applicable to all ships in the area 0° to 30°, area 0° to 40°, area 30° to 40°, max GZ at 30° or greater, angle of maximum GZ. The criteria contained in the reference are presented in Table 2.

Table 2. IMO criteria A.749(18) Ch3

Criteria	Value
Area 0° to 30° (m.rad)	≥ 0.055
Area 0° to 40° (m.rad)	≥ 0.09
Area 30° to 40° (m.rad)	≥ 0.03
Max GZ at 30 or greater (m)	≥ 0.2
Angle of maximum GZ (deg)	≥ 25

2.4 Seakeeping

Seakeeping is a simulation to determine the ship's motion due to forces from outside the ship. Seakeeping movement has translational motion, which includes heave, sway and surge, and rotational motion, which provides for pitch, roll, and yaw [12]. Seakeeping can be processed using variations in the average heading angle, while maneuvers can be completed using constant time intervals [11]. The seakeeping simulation uses three ship movements consisting of movements, namely heave, pitch, and roll. Seakeeping also calculates the Response Amplitude Operator (RAO) to determine the amplitude of the ship's response and the angular or translational motion regarding speed transfer and

ship acceleration [7]. The seakeeping equation of motion based on Newton's second law is 6 degrees of freedom (Fig. 12) which is stated as follows [12].

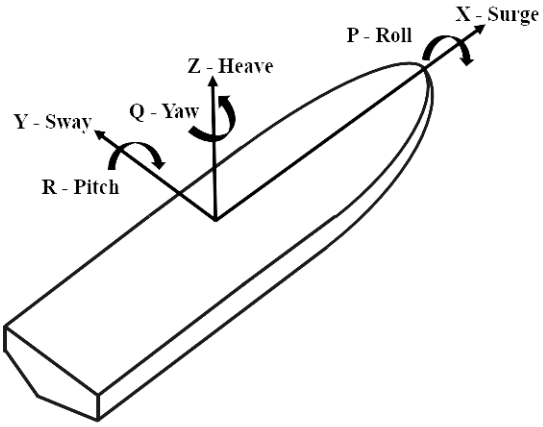

Fig. 12. Six degrees of freedom of ship motions

2.4.1 Heave Motion

Heave motion is the up and down movement of the ship in the direction of the Z-axis due to the crashing wave force. The vertical movement can threaten the safety and efficiency of ship operations [37]. The heave motion in a wave can be determined by the following Eq. 10.

$$\left(M_z + A_z\right)\ddot{z} + \beta_z \dot{z} + a_z z = Z\left(\eta, \psi\right) \tag{10}$$

2.4.2 Pitch Motion

Pitch motion is the movement of the ship parallel to the Y axis. Pitch motion is caused by waves and creates a height difference between the fore and aft of the ship [38]. The pitch motion in the wave can be determined by the following Eq. 11.

$$\left(I_{yy} + A_\theta\right)\ddot{\theta} + \beta_\theta \dot{\theta} + a_\theta \theta = \theta\left(\eta, \psi\right) \tag{11}$$

2.4.3 Roll Motion

Roll motion is a movement around the X-axis caused by waves from the left or right side of the ship. Roll motion is most related to the stability of the ship so that it affects the comfort of passengers and safety of navigation [39]. The pitch motion in the wave can be determined by the following Eq. 12.

$$\left(I_{xx} + A_\phi\right)\ddot{\phi} + \beta_1 \dot{\phi} + \beta_2 \dot{\phi}\left|\dot{\phi}\right| + \beta_3 \phi^3 + g\Delta GZ = M\left(\eta, \psi\right) \tag{12}$$

2.5 Motion Sickness Insidence

Reflected sea waves will cause the ship to shake, causing passengers to get motion sickness when the ship is sailing [28]. The comfort of the ship for the crew needs to be considered when facing extreme weather and big waves. The intensity of drunkenness of passengers should also be minimized because apart from the crew of the ship, there will also be other passengers carrying out the rescue. Motion Sickness Incidence (MSI) was developed by the US Navy in the early 1970s to investigate passenger responses to various ship motions, such as vertical sinusoidal of multiple amplitudes [7]. Seasickness is a problem that is influenced by the speed of the ship and the duration of sailing. The percentage of drunkenness during a two-hour navigation can be expressed in Eq. 13 [40].

$$MSI = 100\left[0.5 + erf\left(\frac{\log_{10}\left(\frac{WVA}{g}\right) - \mu MSI}{0.4}\right)\right] \tag{13}$$

WVA is the average value of vertical acceleration a_v at 40 m in front of the center for a total mass *N* using Eq. 14.

$$WVA = \frac{1}{N}\sum_{i=1}^{N}\left|\alpha_v\left(t_i\right)\right| \tag{14}$$

μ_{MSI} can be found using Eq. 15.

$$\mu MSI = -0.819 + 2.32(\log_{10} \omega_e)^2 \quad (15)$$

2.6 Deck wetness

The speed of a ship and the intensity of strong winds will be directly proportional to the probability of wetness of the deck [24]. Deck wetness is also one of the seakeeping characteristics that need to be considered because it will affect the waterline structure with the wetness of the deck [13]. The wetness of the deck occurs, among others, due to the relative vertical movement that exceeds the ship's draft [13]. Deck wetness value needs to be suppressed to get the lowest possible deal so that the ship's stability level is maintained. Deck wetness makes decks wet, which can be dangerous for crew and cargo [41]. So, the deck wetness needs to be minimized to keep the ship awake. The following equation defines the probability of deck wetness using Eq. 16.

$$P(deckwetness) = \exp\left(\frac{-f_e^2}{2m_0}\right) \quad (16)$$

2.7 Floodable length curve

In designing a design, apart from looking for criteria to support the performance of the ship, it is also necessary to prevent ship accidents. A shipwreck is an unexpected and unwanted thing when sailing. Leaks can be prevented to minimize casualties when an accident occurs. Floodable length analysis prevents the sinking of the margin line after entering the ship so that the boat does not sink. Floodable length is the length of the allowable leakage curve when a compartment has a leak [42]. The length of the floodable length curve will adjust to the effects of displacement and permeability of the compartment. The ship's flood margin line is a minimum of 76 millimeters (3 inches) below the ship's highest transverse bulkhead deck [43]. Analysis of the length of the floodable prevents the sinking of the margin line after entering the ship so that the ship does not sink [44]. The following linear interpolation can find the flood length from the endpoint using Eq. 17.

$$I = I' + \frac{v_c - v'_c}{v''_c - v'_c}(I'' - I') \quad (17)$$

The calculation only considers the longitudinal distance from the afterpeak to the forepeak. To calculate the total, it is by adding the flood length with the back end with afterpeak and the front end with forepeak [43] using Eq. 18.

$$I_{APtoendpoint} = I + \alpha \quad (18)$$

$$I_{FPtoendpoint} = I + \beta \quad (19)$$

2.7.1 Bulkhead

Bulkhead is an essential part of preventing ship flooding. The bulkhead divides the ship into several compartments to limit the length of the flood for each location so as not to exceed the allowable limit [43]. Bulkhead cannot fully guarantee that the ship will not sink like on the Titanic, where the hull is open, and the water enters for a long time [44]. Each bulkhead has its level of permeability in accepting incoming water capacity. Permeability is the ratio that can be filled by water and can be determined by Eq. 20.

$$\mu = \frac{v_t}{v_c} \quad (20)$$

The volume of flooding entering the ship can be calculated by Eq. 21.

$$v_t = \nabla_t - \nabla_0 \quad (21)$$

2.8 State of Art

This research was conducted using several methods and calculations from several previous studies. This research is also aimed at developing existing research into more complex ones. Research on criteria on ships has been carried out using several methods. Table 3 shows that each criterion will affect the ship's performance when sailing from internal and external factors [52-57]. Research with several criteria at once, such as resistance, stability, seakeeping, Motion Sickness Incidence, Deck wetness, and Floodable length, is still little done. Therefore, this research was conducted to design a fast patrol boat with several criteria to get optimal results. In addition to analyzing the ship's design to obtain optimal results, it is also necessary to analyze external factors and anticipate accidents. Some numerical studies on ships that have been carried out are shown in Table 3.

Table 3. Previous numerical research on ship simulation.

No	Author (Year)	Title	Calculation Method	Conclusions
1	Khai et al. [29]	A Comparison Study On the Resistance Calculation of Planning Boat	The savitsky method and the Reynold Average Navier Stokes Equation (RANSE) CFD method	The simulation results show that the Savitsky method is more accurate in calculating the trim angle and the initial process of calculating the resistance with a fast procedure. In contrast, the CFD method in calculating ship resistance is accurate and thorough, but the process is quite long.
2	Julianto et al. [30]	Investigation of Hull Design To Quantify Resistance Criteria Using Holtrop's Regression-Based Method and Savitsky's Mathematical Model: A Study Case of Fishing Vessels	The savitsky method and Holtrop's regression-based method	The addition of fins makes the ship's resistance smaller in both the Savitsky and Holtrop methods. With the addition of fins, the difference is obvious at high speeds, which makes the error rate smaller than at low speeds.
3	Nam-Kyun and Hun [45]	A Quantitative Methodology for Evaluating the Ship Stability Using the Index for Marine Ship Intact Stability Assessment Model	Empirical method (IMSISA model) and IMO intact stability regulations	The IMSISA model used shows the results of meeting the stability index with 100% accuracy, where the model is better than the previous model.
4	Woo et al. [46]	Analysis of the Relationship between GM and IMO Intact Stability Parameters to Propose Simple Evaluation Methodology	the Simple Evaluation Methodology for Intact Stability (SEMIS) and IMO Intact Stability Regulations	SEMIS consists of four phases (Calculating GM, Calculating Parameters, Evaluating Parameters, and Stability Assessment, respectively) using 28 loading conditions, two ship models of 336 loading conditions, and 19 models on stability parameters. The analysis shows that SEMIS is a safe and easy method for ship crews to evaluate ship stability conditions.
5	Yao et al. [47]	Numerical investigation of side-wall effects on the seakeeping performance of a ship advancing in waves	Numerical methods and metode LFS-DB	Calculations using the numerical method on the side walls of non-penetrating ships produce high efficiency and accuracy. Hydrodynamic analyses using the numerical method and LFS yielded satisfactory results with experimental results.
6	Wang et al. [48]	Seakeeping optimization of trimaran outrigger layout based on NSGA-II	Metode 2.5D (Numerical Method)	The layout of the outrigger affects the heave, pitch, and roll motion of the ship during head-sea waves. The placement of the RAO wave amplitude also involves the laying of conditional outriggers depending on the speed and the waves that occur.

No	Author (Year)	Title	Calculation Method	Conclusions
7	Scamardella et al. [49]	Passenger ship seakeeping optimization by the Overall Motion Sickness Incidence	Lackenby method	Optimizing the heave, pitch, and roll values of RAOs seakeeping are aimed at maximizing the health of passengers on board. Prismatic coefficient variation and buoyancy center position to get optimal seakeeping value.
8	Dhavalikar et al. [50]	Development of Empirical Formulation for Bow Flare Slamming and Deck Wetness for Displacement Vessels	Empirical method	Speed is a factor that significantly affects water pressure. Freeboard indicates that the deck will be waterlogged if the water rises statically and considers dynamic conditions.
9	Kałkowska [43]	Floodable length of a bulk carrier	Shirokauer's method	The resulting graph shows the compartment when there is a flood. There is a dangerous and safe compartment in the event of a leak.
10	Pennanen et al. [51]	Application of Vessel TRIAGE for a Damaged Passenger Ship	The Vessel TRIAGE method	Heeling angle is the "s-factor" that determines the TRIAGE value of the ship with color code stability. In addition to the stability threat factor, this method can calculate the flood level based on the floodable length curve.

Khai et al. [29] used the boat model C1 in the Naples series to analyze the ship's resistance using the methods used, namely the Savitsky method and the CFD method. The resulting analysis shows that the Savitsky method has advantages in the initial process of calculating resistance with a simple and fast process. Besides that, it is more accurate in estimating the trim angle differs by 0.23% while the CFD differs by 10%. The CFD method has advantages in calculating the total resistance, which is accurate and thorough with a different value of 2%, while the Savitsky method is 10%. Julianto et al. [30]. used the Savitsky method and Holtrop's regression-based method with variations in the addition of fins on the ship. The addition of fins affects the ship by reducing the total resistance. From numerical calculations and the Savitsky method, it has a difference of 14%, and the Holtrop method has a difference of 2%. Nam-Kyun and Hun [45] proposed the IMSISA method to calculate stability efficiently and quantitatively. The calculation model consists of a numerical stability index and ship safety stability with 32 ship loading scenarios. The method's accuracy is 100% against the IMO stability standard and is better than the previous study, only having an accuracy of 84.4%. Woo et al. [46] proposed the SEMIS method to evaluate the intact stability of IMO with GM parameters. Using 28 loading conditions and two ship models from 336 loading conditions and 19 models on stability parameters with four phases, namely calculating GM, calculating parameters, evaluating parameters, and evaluating stability in sequence. SEMIS calculations show that the four loading conditions and 28 scenarios are by the IMO intact stability standard. Yao et al. [47] developed a method to calculate seakeeping performance on sidewall effects under non-penetrating conditions and produce more efficient and accurate values. Using the Lewis form ship resulted in good and satisfactory numerical calculations and experiments.

Wang et al. [48] tested the trimaran model on heave, pitch, and roll movements to determine the relationship between the vertical motion of the ship and the ward speed, wavelength, and outrigger layout. The results show that the location of the outrigger and the direction of the waves affect the amplitude of RAOs, heave, pitch, and roll. Scamardella et al. [49] analyzed the Motion Sickness Incident (MSI) criteria with operating scenario parameters and wave spectrum. Using several types of the hull with the parameters of the center of buoyancy and Froud number are the same and using the JONSWAP wave spectrum. The variations used can optimize the value of Heave, pitch, and roll and improve the health of passengers on board. Dhavalikar et al. [50] calculated the pressure of slamming bow flare and green water load using empirical methods. Takes into account marine weather conditions with flare angles and waterlines. The velocity factor will affect the water pressure, and the freeboard will be flooded if the water rises statically by considering dynamic conditions. Limiting the waterline with 2D numerical simulation can be a solution to overcome the problem of overpressure. Kałkowska [43] investigated the volume of the compartment when it was inundated without causing the ship to sink. The resulting graph shows the condition of the compartment when there is a flood. There is a dangerous compartment in case of a leak and requires special handling. There is also a compartment that is safe from leakage. Even if an adjacent compartment leaked, the ship would not sink. Most ships are double-skinned to prevent vessel leakage, according to IMO standards. Pennanen et al. [51] used the TRIVAGE

method to classify the severity of ships against flooding. Heeling angle is the "s-factor" that determines the ship's TRIAGE value with a stability color code where the stability threat factor turns yellow when the heel exceeds 12° and red when the heel exceeds 15°. In addition to the stability threat factor, this method can calculate the flood level based on the floodable length curve.

3 METHODOLOGY

This study uses several V-shaped hull designs, which are analyzed to get a design with optimal performance. Using the approach method with comparison vessels to get the best hull shape. The method does not require complicated calculations because the reference ship used has been designed and designed by the company and expert designers [52]. Using Maxsurf Modeler software in making the hull design concerning the original ship dimensions. The design is simulated using Maxsurf Resistance, Maxsurf Stability, and Maxsurf Motion software according to the simulated factors and criteria. The addition of bulkhead is carried out on a floodable length simulation with several variations in distance. From the result data, some of these factors will be compared to be taken to be the best and most feasible design to be realized. The data results also need to be validated with the applicable IMO standards to ensure the safety of the design later.

3.1 Ship Data

The design is designed using the main dimensions that have been determined regarding the original ship. Nine designs were made to obtain varied data results to obtain an optimal design. In addition to the main sizes for different vessels, different hull shapes of the same type are also used (see Table 4). The designed hulls are a single chine hull and semi-displacement hull, multi-chine hull and planning hull, single chine hull and planning hull with a smaller curved planning area. The reference ships used include the NSW WATER POLICE - Class 1 reference Design 1, the AUSTAL INSHORE Patrol 21 (Det Norske Veritas - DNV) reference Design 2, the DASTOOR AUSTAL Patrol 22 (Lloyd's Register - LR) reference Design 3, the Patrol Emergency Response Vessel (ERRV) reference Design 4, Coast Guard Sport Pilot Boat reference Design 5, Offshore Pilot/Patrol Boat reference Design 6, Grandweld Shipyard Delivers 21M Discovery Class Vessel Fujairah Pilot I reference Design 7, EP116 20 m Pilot boat reference Design 8, 20M PATROL BOAT VCSM-Class reference Design 9. The design process begins with designing the lines plan of each design and then creating a 3D design. The results of the 3D designs that have been made are shown in Fig. 13.

Table 4. Principal dimension of fast patrol boat designs.

Parameters	Value								
	Design 1	Design 2	Design 3	Design 4	Design 5	Design 6	Design 7	Design 8	Design 9
Length Overall (m)	21.2	21.2	21.6	20.8	21.163	21.95	21.3	20.5	20
Depth (m)	3.3	2.8	3.6	2.95	2.914	2.74	2.89	2.92	2.89
Draft (m)	1.7	1.83	1.5	1.2	1.653	1.22	1.15	1.5	1.49
Beam (m)	5.5	5.5	6	5.5	6.34	5.49	5.6	5.9	5.29
Length Waterline (m)	19.761	20.303	19.633	18.719	19.829	19.960	19.328	19.140	18.680
Displacement (t)	56.83	79.02	42.792	27.65	65.65	32.85	30.85	55.54	48.47
Block Coefficient (-)	0.346	0.401	0.339	0.384	0.376	0.396	0.378	0.375	0.375
Ratio LOA - Beam (-)	4.025	3.812	4.580	5.821	3.714	5.831	5.249	3.699	4.008
Ratio Beam - Depth (-)	2.888	2.910	2.858	2.681	3.232	2.808	3.202	3.449	3.128

Note:

1. Design 1 - NSW WATER POLICE - Class 1
2. Design 2 - AUSTAL INSHORE Patrol 21
3. Design 3 - DASTOOR AUSTAL Patrol 22
4. Design 4 - Patrol Emergency Response Vessel
5. Design 5 - Coast Guard Sport Pilot Boat
6. Design 6 - Offshore Pilot/Patrol Boat
7. Design 7 - Grandweld Shipyard Delivers 21M Discovery Class Vessel Fujairah Pilot I
8. Design 8 - EP116 20 m Pilot boat
9. Design 9 - 20M PATROL BOAT VCSM-Class

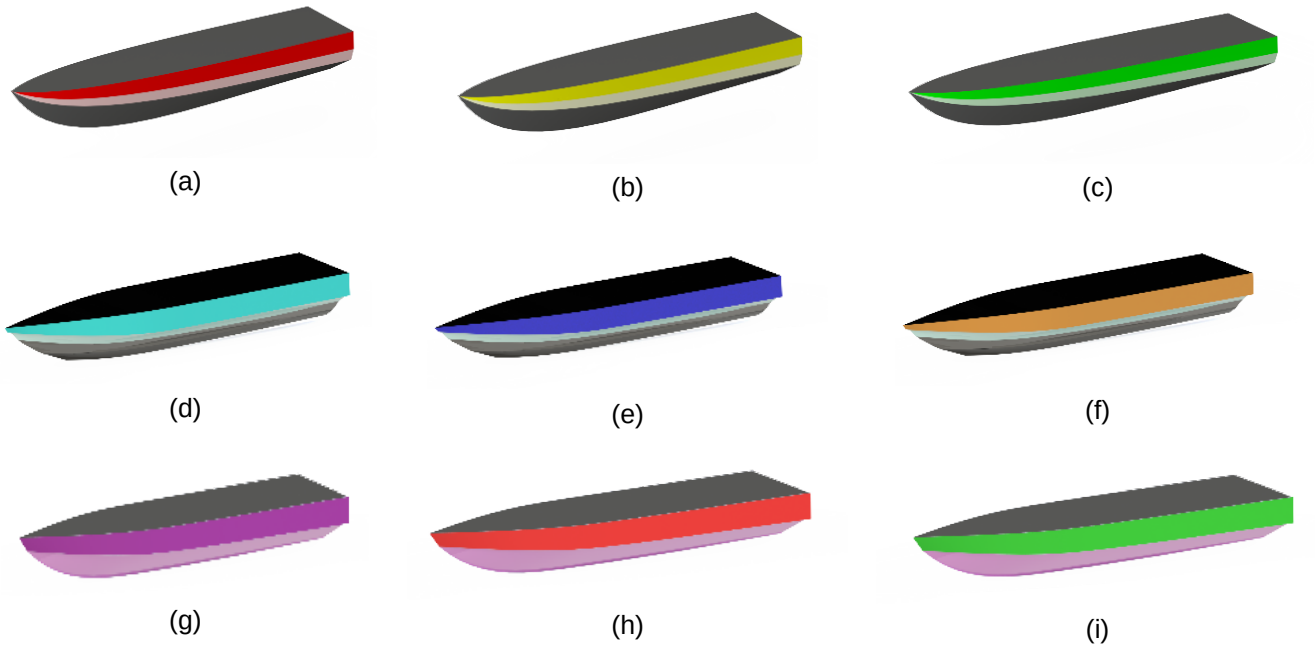

Fig. 13. 3D hull design: (a) Design 1; (b) Design 2; (c) Design 3; (d) Design 4; (e) Design 5; (f) Design 6; (g) Design 7; (h) Design 8; and (i) Design 9

From the design variations that have been carried out, adding a waterproof bulkhead during the floodable length simulation is intended to obtain results against leakage. In addition to the variations added to the simulation, the control variables are also used for each criterion. Each criterion is given a control variable to later prevent bias in the calculation.

3.1.1 Research Parameter

The variables used in each simulation consist of two variables: the control variable and the independent variable. The control variable is the reference variable for each criterion during the simulation, and the independent variable is to get the desired variation. Each criterion uses different variables to simulate both control and independent variables. In addition to the variables, each criterion uses methods and regulations or standard values that determine the feasibility of the fast patrol boat design later. One of the methods used is the Savitsky method in resistance simulation. The regulation or standard that will be used is the IMO (International Maritime Organization) standard which is the supervisory body for safety and security in shipping.

The ship's calculation uses the Savitsky method with the control variable, namely the Froude number. The route number value used in this resistance simulation is 0 to 2.217, which, when converted to speed, ranges from 0 to 60 knot in Design 1, which is the reference. In stability testing using IMO (International Maritime Organization) standard reference A.749(18) Ch3 - Design criteria applicable to all ships in area 0° to 30°, area 0° to 40°, area 30° to 40°, max GZ at 30° or greater, angle of maximum GZ. The results obtained will later be validated with the provisions of the value that must be achieved to determine whether the ship passes or not. After knowing the initial stability criteria, the simulation determines the ship's response when getting an external force. Seakeeping analysis will analyze the ship's heave, pitch, and roll motion with wave angles of 90°, 135°, and 180°. From the effect of the waves that occur, it will undoubtedly affect the condition of the crew on the ship and the level of wetness on the deck due to the brunt of the waves. It is also simulated to determine crew response and deck conditions in MSI (Motion Sickness Incidence) and deck wetness simulations. This analysis uses variable control waves with a height of 0.1 m, 0.3 m, and 0.5 m, and the average wave in Indonesia is 1.875 m. In the simulation of preventing the leakage or floodable length using three variations of the partition distance and the same permeability level starting from 85% - 95% according to the room. This simulation determines the length of the leak arm against the size of the compartment position. The permeability level of each compartment is shown in Table 5, and the distance length variation for each bulkhead can be seen in Table 6.

Table 5. Permeability levels of each compartment.

Compartment	1	2	3	4	5	6
Value Permeability (%)	95	85	98	95	95	95

Table 6. Length of bulkhead variation in design.

Variation	Bulkhead				
	Range 1	Range 2	Range 3	Range 4	Range 5
Variation 1	3.7 m	5.0 m	8.6 m	13.5 m	17.7 m
Variation 2	3.8 m	8.5 m	13.4 m	15.3 m	17.7 m
Variation 3	2.2 m	3.4 m	8.1 m	15.8 m	18.2 m

4 RESULT AND DISCUSSION

4.1 Ship Resistance

This resistance calculation produces several results, including a comparison between the Froude number value and the resistance value, as well as the Froude number value and power requirements. So from the nine designs tested, the best design in resistance testing can be seen. The resistance results are shown in Tables 7 to 9, as well as a comparison graph between the resistance value and the Froude number value and power requirement in Fig. 14 and 15.

Table 7. Resistance and power hull results from Design 1 to Design 3.

No.	Froude Number LWL (-)	Savitsky planning resistance (N)					
		Design 1		Design 2		Design 3	
		Resistance (N)	Power (W)	Resistance (N)	Power (W)	Resistance (N)	Power (W)
1	0	0	0	0	0	0	0
2	0.554	56817.81	487160.15	89474.34	777132.69	36009.66	307576.22
3	0.924	73833.56	844072.53	113786.21	1318376.2	47566.68	541965.31
4	1.293	90284.68	1290179.24	135131.22	1957612.95	59778.02	851604.22
5	1.663	101135.12	1734280.04	145414.64	2528335.85	70079.41	1198207.08
6	2.033	107168.02	2144021.85	147976.48	2999774.56	77617.86	1547290.51
7	2.217	111694.4	2553802.87	148585.27	3443061.43	83871.96	1911192.86

Table 7 shows the results of the calculation of the resistance and power required in Design 1, Design 2, and Design 3. At the smallest Froude number value, namely 0.554, Design 1 has a resistance value of 56817.81 N and a power of 487160.15 W, Design 2 has a resistance value of 89474.34 N. and power of 777132.69 W, and Design 3 has a resistance value of 36009.66 N and a power of 307576.22 W. At the Froude number value of 2.217, Design 1 has a resistance value of 111694.4 N and a power of 2553802.87 W, Design 2 has a resistance value of 148585.27 N and a power of 3443061.43 W, and Design 3 has a resistance value of 83871.96 N and a power of 1911192.86 W.

Table 8. Resistance and power hull results from Design 4 to Design 6

No.	Froude Number LWL (-)	Savitsky Planing Resistance (N)					
		Design 4		Design 5		Design 6	
		Resistance (N)	Power (W)	Resistance (N)	Power (W)	Resistance (N)	Power (W)
1	0	0	0	0	0	0	0
2	0.554	19275.91	160766.62	68865	591122.77	23512.55	202498.81
3	0.924	25254.02	280954.64	88763.04	1016320.71	31014.11	356293.74
4	1.293	31790.32	442203.55	106530.5	1525135.08	39230.26	563497.97
5	1.663	37951.15	633589.31	116295.27	1998303.51	47015.97	810536.82
6	2.033	43010.4	837191.64	120577.05	2415593.61	53461.15	1074595.13

No.	Froude Number LWL (-)	Savitsky Planing Resistance (N)					
		Design 4		Design 5		Design 6	
		Resistance (N)	Power (W)	Resistance (N)	Power (W)	Resistance (N)	Power (W)
7	2.217	47273.51	1051849.47	123660.32	2831847.03	58914.39	1353630.72

The results of the analysis of resistance and power in Design 4 to Design 6 are shown in table 8. The analysis results show that Design 4 on Froude number 0.555 has a resistance of 19275.91 N and a power of 160766.62 W, the largest Froude number value is 2.217, Design 4 has a resistance value of 47273.51 N and a power of 1051849.47 W. In Design 5, with the smallest Froude number value of 0.554, Design 5 has a resistance of 68865 N and a power of 591122.77 W. At the largest Froude number value of 2.217, Design 5 has a resistance value of 123660.32 N and a power of 2831847.03 W. The results of Design Analysis 6 show that the Froude number 0.555 has a resistance of 23512.55 N and a power of 202498.81 W, and the largest Froude number value is 2.217. Design 4 has a resistance value of 58914.39 N and a power of 1353630.72 W.

Table 9. Resistance and power hull results from Design 7 to Design 9

No.	Froude Number LWL (-)	Savitsky Planing Resistance (N)					
		Design 7		Design 8		Design 9	
		Resistance (N)	Power (W)	Resistance (N)	Power (W)	Resistance (N)	Power (W)
1	0	0	0	0	0	0	0
2	0.554	21810.13	184832.47	51439.82	433815.65	44180	368095.11
3	0.924	29326.06	331520.34	66364.03	746541.23	57107.79	634679.65
4	1.293	37466.96	529582.28	80289.36	1129308.65	69937.85	971836.46
5	1.663	45163.32	766180.51	88985.16	1502227.89	78928.44	1316346.19
6	2.033	51709.15	1022768.04	93710.07	1844462.01	84189.39	1637050.71
7	2.217	57548.84	1301136.78	97534.51	2194423.35	88199.04	1960437.92

Table 9 shows the results of the calculation of the resistance and power required in Design 7, Design 8, and Design 9. At the smallest Froude number value, namely 0.554, Design 7 has a resistance value of 21810.13 N and a power of 184832.47 W, Design 8 has a resistance value of 51439.82 N. and a power of 433815.65 W, and Design 9 has a resistance value of 44180 N and a power of 368095.11 W. At the Froude number value of 2.217, Design 7 has a resistance value of 57548.84 N and a power of 1301136.78 W, Design 8 has a resistance value of 97534.51 N and a power of 2194423.35 W, and Design 9 has a resistance value of 88199.04 N and a power of 1960437.92 W.

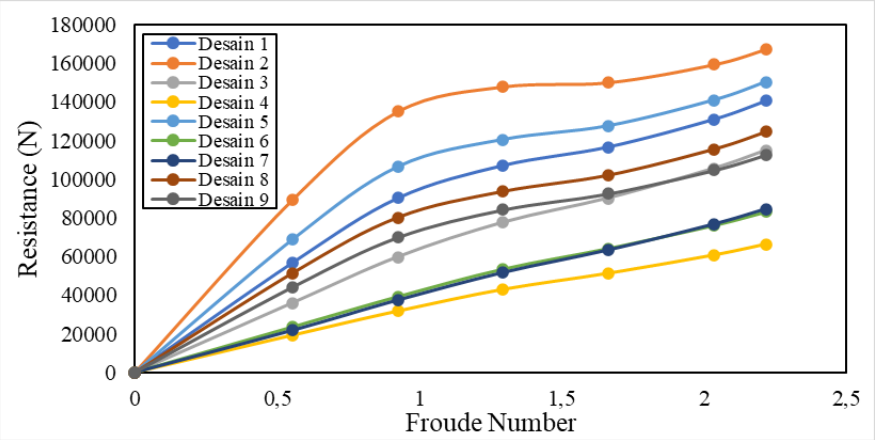

Fig. 14. Resistance simulation: Graph of the relationship between Froude Number and Resistance

The resistance graph of the simulation results in Fig. 14 shows that the resistance value is directly proportional to the Froude number value. Of the nine designs, the results show different lines between the Froude number and Resistance comparisons. Design 4, Design 6, Design 7, and Design 3 steadily increase from the smallest Froude number value to the largest Froude number. In Design 9, Design 8, Design 1, Design 5, and Design 2, the resistance value also increased to the Froude number value. Still, the increase was quite significant in the initial value compared to when the middle value reached the largest value.

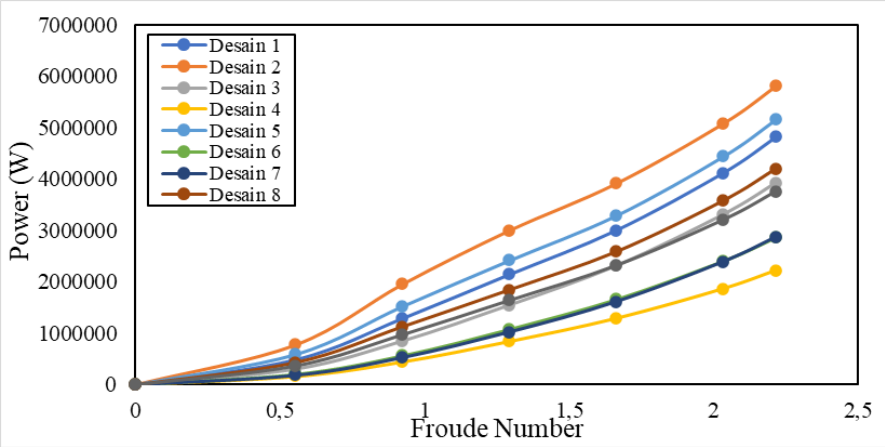

Fig. 15. Resistance simulation: Graph of the relationship between Froude Number and Power

Fig. 15 shows a graph of the relationship between Froude number and Power in nine simulation designs. The power value is directly proportional to the increase in the Froude number value. No one has experienced a decreased power when the Froude number value gets bigger. The value of nine Designs also experienced a fairly steady increase. The smallest power value is in Design 4, while the largest is in Design 2.

Resistance and power have a value that is directly proportional to speed. It is known that the higher the speed of the ship, the higher the resistance and power required. The design that has the smallest value is Design 4, with a maximum resistance value of 47273.51 N and power of 1051849.47 W. The design that has the most significant resistance value is Design 2, with a maximum resistance value of 148585.27 N and power of 3443061.43 W. From the data obtained, it is also known that the differences in the main size of the ship and the analyzed hull shape will affect the value of the resistance and power requirements of the ship.

The results of the resistance simulation data obtained a more efficient and less efficient design for resistance. The three designs that have the smallest values are Design 4, Design 6, and Design 7. The design has the smallest and most efficient value compared to the others, with a minimum resistance value of 19275.91 N and a maximum resistance value of 66460.23 N, with the smallest power requirement with a minimum value of 160766.62 W and a maximum rating of 2218101.42 W. From the Fig. 14 and the Fig. 15, Design 6 and Design 7 produce intersecting graphs so that it can be seen that there is a more efficient design at low speeds and reduced efficiency at high speeds, and vice versa. From the data obtained, Design 7 is more efficient at low speeds, but at high speeds, it is more efficient than Design 6.

4.2 Large Angle Stability of ship

Large angle stability is one of the factors used in testing the safety factor in the designed design. IMO (International Maritime Organization) Standard A.749(18) was tested on nine designs that were designed. The results of the large angle stability test are presented in Table 10.

Table 10. data results of large angle stability of ship

Design	Criteria				
	Area 0° to 30° (m.rad)	Area 0° to 40° (m.rad)	Area 30° to 40° (m.rad)	Max GZ (m)	Angle of Maximum GZ (deg)
Design 1	0.09	0.16	0.07	0.49	51.8
Design 2	0.16	0.25	0.09	0.52	33.6
Design 3	0.056	0.113	0.057	0.725	60.9
Design 4	0.0718	0.1702	0.0984	0.949	56.4
Design 5	0.2285	0.3713	0.1428	0.847	40.9
Design 6	0.1226	0.2395	0.1169	0.903	52.7
Design 7	0.1515	0.278	0.1265	0.984	52.7
Design 8	0.2165	0.3508	0.1343	0.824	43.6
Design 9	0.1731	0.28	0.1069	0.668	45.5

Based on the design stability tests, nine passed or met the criteria in Table 10. In the criteria Area 0° to 30°, the nine designs exceed 0.055 m.rad. In the criteria for Area 0° to 40°, the nine designs also meet the criteria by having a value above the specified standard of 0.09 m.rad. In the criteria for Area 30° to 40°, the nine designs also meet the standard value set at 0.03 m.rad. The ninth also met the GZ maximum arm length criteria with a standard value of 0.2 m. The last criterion on stability is the angle of maximum GZ with a standard of 25°.

The stability data obtained shows that the three designs with the best GZ maximum arm length are Design 4, Design 6, and Design 7. At the angle of maximum GZ, which has the largest angle, namely Design 3, Design 4, and two designs that have the same value. Namely, Design 6 and Design 7. So that it can be seen that Design 4 is a stability simulation which is one design that has a high level of stability with a maximum GZ arm length of 0.949 m and an angle of maximum GZ of 56.4°. In addition, there is Design 7, which has a maximum GZ arm length of 0.984 m and a GZ angle of maximum value of 52.7°. There is also Design 6 which has a maximum GZ arm length of 0.903 m and a GZ angle of maximum value of 52.7°. From the stability results, it can also be seen that the main size of the ship and the value of the ship's displacement affect the level of ship stability where there are ships that have a large GZ maximum arm length value but a small GZ angle of maximum value.

4.3 Seakeeping

The performance of a fast patrol boat at high speed will undoubtedly be affected by waves. The wave characteristics are based on the Meteorology, Climatology, and Geophysics Agency (BMKG), with an average wave height of 1.875 m. The angle of incidence of waves uses three angles of incidence, namely 90°, 135°, and 180°, with the confluence of heave, pitch, and roll waves. The jam also uses speeds of 10 knot, 20 knot, and 30 knot. The angle of incidence of the wave is shown in Fig. 16. The results of the simulation will show the Response Amplitude Operator (RAO) function with the movement frequency and counter frequency to determine the frequency of the waves hitting the ship.

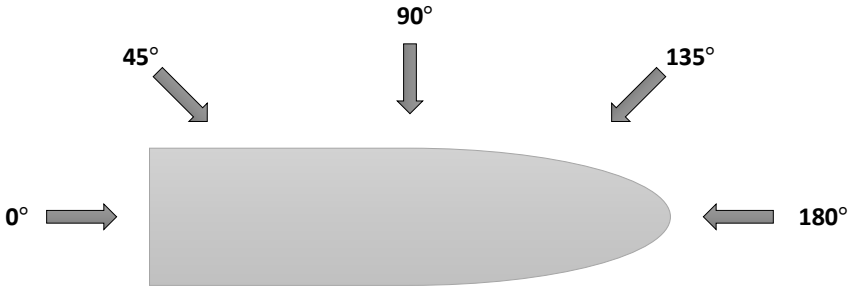

Fig. 16. Definition of the angle of incidence of the wave

4.3.1 Heave Motion

The simulation results of seakeeping heave motion are presented in Fig. 17 to Fig. 19 as a graph between RAO and Counter Frequency. Fig. 17 to Fig. 19 is a heave graph at the maximum speed used, which is 30 knots, with a wave angle of 90°, 135°, and 180°.

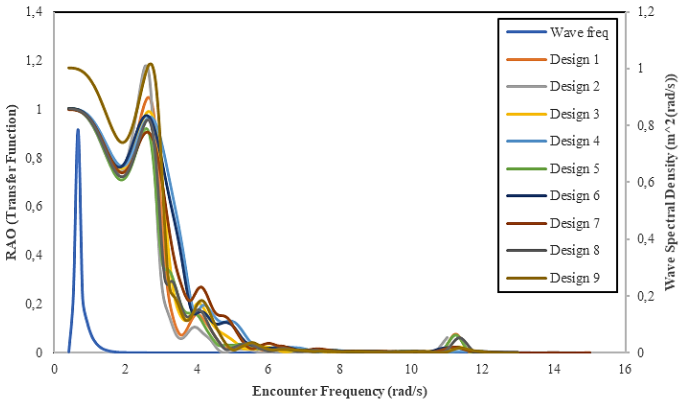

Fig. 17. RAO transfer function heave motion angle of incident wave 90°

Fig. 17 shows a heave motion graph of the effect of a wave force with an angle of incidence of 90° and a speed of 30 knots. It is known that the peak wave frequency with the nine designs is almost the same but differs in the encounter frequency. Peak wave frequency during encounter frequency is 0.65 rad/s, and wave spectral density is 0.91 m²s/rad. Design 7 has the smallest peak value with an encounter frequency of 2.6 rad/s and a wave spectral density of 0.9 m²s/rad. The highest peak is in Design 9, with an encounter frequency of 2.6 rad/s and a wave spectral density of 1.01 m²s/rad.

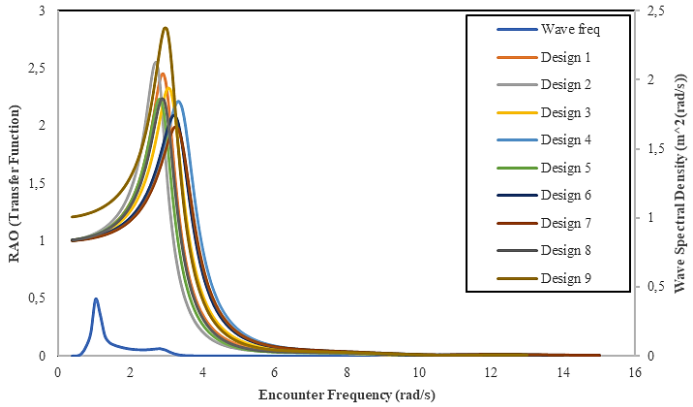

Fig. 18. RAO transfer function heave motion angle of incident wave 135°

Fig. 18 shows a heave motion graph of the effect of a wave force with an angle of incidence of 135° and a speed of 30 knots. It is known that the wave frequency peaks are much smaller than the design nine peaks and differ in the encounter frequency. Peak wave frequency when encounter frequency is 1 rad/s, and wave spectral density is 0.49 m²s/rad. Design 7 has the smallest peak value with an encounter frequency of 3.2 rad/s and a wave spectral density of 1.98 m²s/rad. The highest peak is in Design 9, with an encounter frequency of 3 rad/s and a wave spectral density of 2.3 m²s/rad.

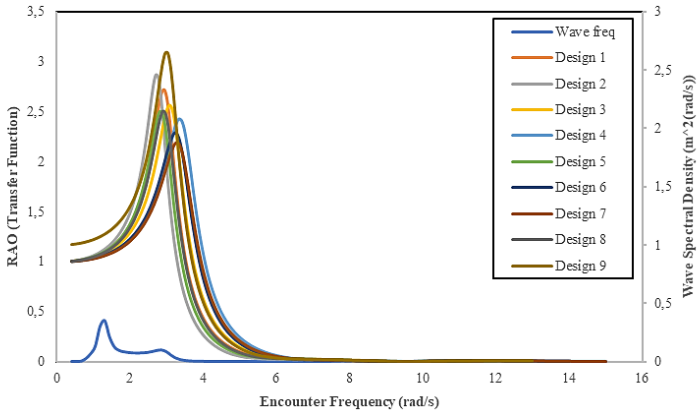

Fig. 19. RAO transfer function heave motion angle of incident wave 180°

Fig. 19 shows a heave motion graph of the effect of a wave force with an angle of incidence of 180° and a speed of 30 knots. It is known that the wave frequency peaks are much smaller than the design nine peaks and differ in the encounter frequency. The peak wave frequency during encounter frequency is 1.3 rad/s, and the wave spectral density is 0.41 m²s/rad. Design 7 has the smallest peak value with an encounter frequency of 3.2 rad/s and a wave spectral density of 2.1 m²s/rad. The highest peak is in Design 9, with an encounter frequency of 3 rad/s and a wave spectral density of 2.6 m²s/rad.

The seakeeping simulation results on heave motion show the frequency of wave encounters and the response of the ships up and down movement. From the three angles of incidence in the seakeeping heave motion, all the proposed designs do not experience superposition where the initial and peak values are not tangent to the wave frequency. The peak wave frequency differs from the peak value of the entire model. At 90°, the peak wave frequency when the frequency equalizer is 0.65 rad/s and the peak value of ROA Heave throughout the design is between 2.53 rad/s to 2.7 rad/s. At an angle of 135°, the peak wave frequency when the counter frequency is 1 rad/s and the peak value of ROA Heave throughout the design is between 2.3 rad/s to 3.3 rad/s. At an angle of 180°, the peak wave frequency when the counter frequency is 1.3 rad/s and the peak value of ROA Heave throughout the design is between 2.4 rad/s to 3.3 rad/s. From the three angles of incidence, it is known that the peak of the RAO heave is different from the peak of the wave frequency. So that at the same time, the ship does not receive more than one wave and causes the boat to be more stable.

Fig. 17 shows that at an angle of 90°, the design with the lowest response is Design 7 when the counter frequency is 2.6 rad/s. At a slope of 135°, the design that has the lowest response is Design 7, when the counter frequency is 3.2 rad/s. Meanwhile, at an angle of 180°, the design that has the lowest response is Design 7, when the counter frequency is 3.2 rad/s. So that in this seakeeping heave motion, Design 7 has better stability from up and down movements.

4.3.2 Pitch Motion

Seakeeping pitch motion simulation results are presented in Fig. 20 to Fig. 22 in the form of a graph between RAO and Counter Frequency. Fig. 20 to Fig. 22 is a pitch graph at the maximum speed used, which is 30 knots, with wave angles of 90°, 135°, and 180°.

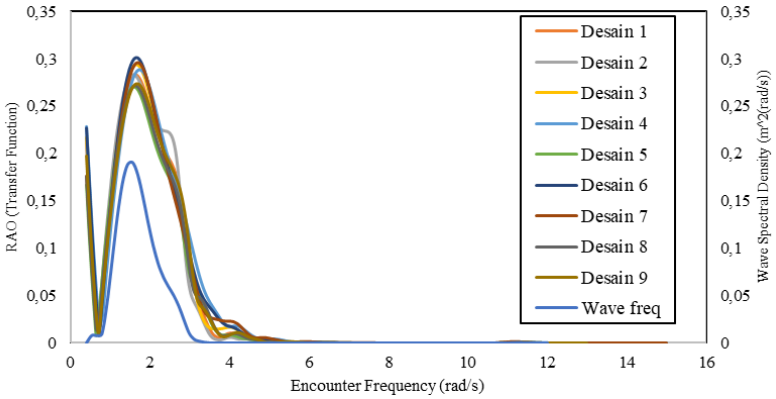

Fig. 20. RAO transfer function pitch motion angle of incident wave 90°

Fig. 20 shows a pitch motion graph of the effect of a wave force with an angle of incidence of 90° and a speed of 30 knots. The graph shows that the wave frequency and RAO in the design are close to each other but do not intersect. The peak wave frequency is smaller, with an encounter frequency of 1.56 rad/s and a wave spectral density of 0.19 m²s/rad. Design 5 has the smallest peak value with an encounter frequency of 1.56 rad/s and a wave spectral density of 0.27 m²s/rad. The highest peak is in Design 6, with an encounter frequency of 1.64 rad/s and a wave spectral density of 0.3 m²s/rad. The peak difference between the hulls is not very significant and quite small.

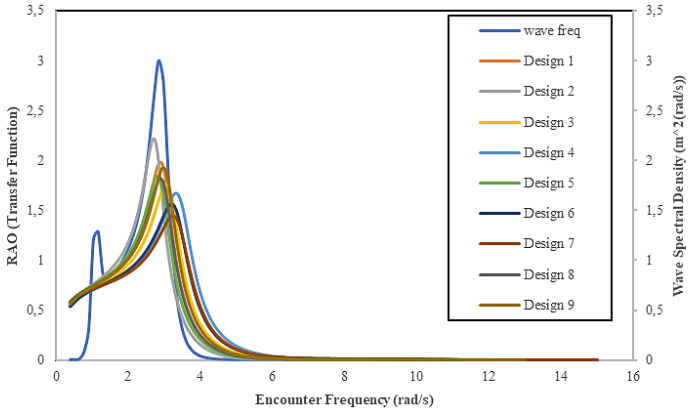

Fig. 21. RAO transfer function pitch motion angle of incident wave 135°

Fig. 21 shows a pitch motion graph of the effect of a wave force with an angle of incidence of 135° and a speed of 30 knots. The graph shows that the wave frequency and RAO in the design are close to each other but do not intersect. The wave frequency has a higher peak than the RAO design, with an encounter frequency of 2.8 rad/s and a wave spectral density of 2.9 m²s/rad. Design 7 has the smallest peak value with an encounter frequency of 3.22 rad/s and a wave spectral density of 1.44 m²s/rad. The highest peak is in Design 2, with an encounter frequency of 2.7 rad/s and a wave spectral density of 2.2 m²s/rad.

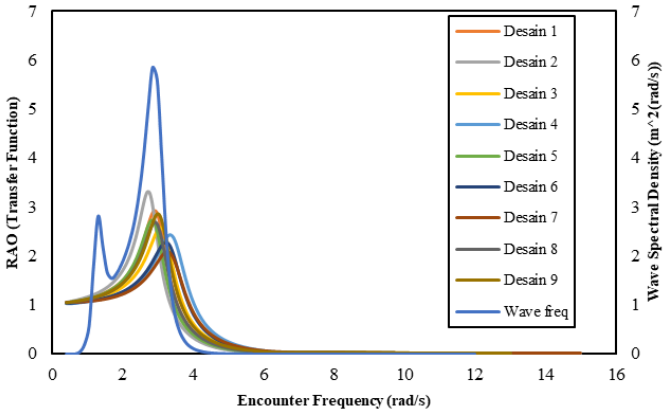

Fig. 22. RAO transfer function pitch motion angle of incident wave 180°

Fig. 22 shows a pitch motion graph of the effect of a wave force with an angle of incidence of 180° and a speed of 30 knots. The graph shows that the wave frequency is higher than the RAO of the nine simulated designs. The peak wave frequency encounter frequency is 2.84 rad/s, and the wave spectral density is 5.85 m²s/rad. Design 7 has the smallest peak value with an encounter frequency of 1.56 rad/s and a wave spectral density of 0.27 m²s/rad. The highest peak is in Design 2, with an encounter frequency of 1.64 rad/s and a wave spectral density of 0.3 m²s/rad. The peak difference between the hulls is not very significant and quite small.

Seakeeping analysis on pitch motion is an analysis of changes in trim on the ship. Overall, the proposed design does not experience superposition conditions from the angle of incidence of waves 90°, 135°, and 180°. This is because the wave frequency and RAO pitch peaks do not intersect. At an angle of 90°, the peak wave frequency when the frequency equalizer is 1.56 rad/s and the peak value of the ROA Pitch of the entire design is between 1.56 rad/s to 1.72 rad/s. At an angle of 135°, the peak wave frequency when the counter frequency is 2.8 rad/s and the peak value of the ROA Pitch throughout the design is between 2.7 rad/s to 3.3 rad/s. At an angle of 180°, the peak wave frequency when the counter frequency is 2.8 rad/s and the peak value of ROA Pitch throughout the design is between 2.7 rad/s to 3.3 rad/s. So innovation can see that the ship does not receive more than two waves which cause the boat to be more stable.

Fig. 20 shows that at an angle of 90°, the design with the lowest response is Design 5 when the counter frequency is 2.7 rad/s. At an angle of 135°, the design that has the lowest response is Design 7 when the counter frequency is 1.4 rad/s. Meanwhile, at an angle of 180°, the design that has the lowest response is Design 7 when the counter frequency is 2 rad/s. So that in this seakeeping pitch motion, Design 7 has better stability from the movement of changing the trim angle, but at an angle of 90°, Design 5 is superior to Design 7.

4.3.3 Roll Motion

The results of the seakeeping roll motion simulation are presented in Fig. 23 to Fig. 25 as a graph between RAO and Counter Frequency. Fig. 23 to Fig. 25 is a rolling graph at the maximum speed used, which is 30 knots, with a wave angle of 90°, 135°, and 180°.

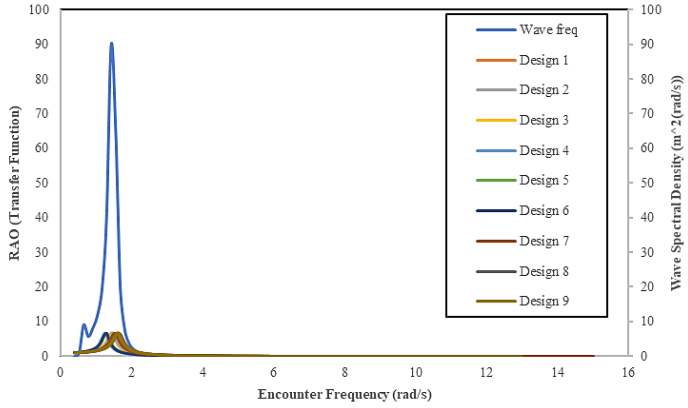

Fig. 23. RAO transfer function roll motion angle of incident wave 90°

Fig. 23 shows a roll motion graph of the effect of a wave force with an angle of incidence of 90° and a speed of 30 knots. The graph shows that the roll motion wave frequency is much higher than the design RAO. The RAO peaks of each design are close together and have almost the same height. Design 3 has the smallest peak value with an encounter frequency of 1.33 rad/s and a wave spectral density of 6.45 m²s/rad. The highest peak is in Design 9, with an encounter frequency of 1.62 rad/s and a wave spectral density of 6.67 m²s/rad. The peak of the wave frequency is the encounter frequency value of 1.43 rad/s and the wave spectral density of 89.7 m²s/rad. The 90° angle of incidence is known to be the angle of incidence that has a high effect on ship roll with a high peak wave frequency and design RAO.

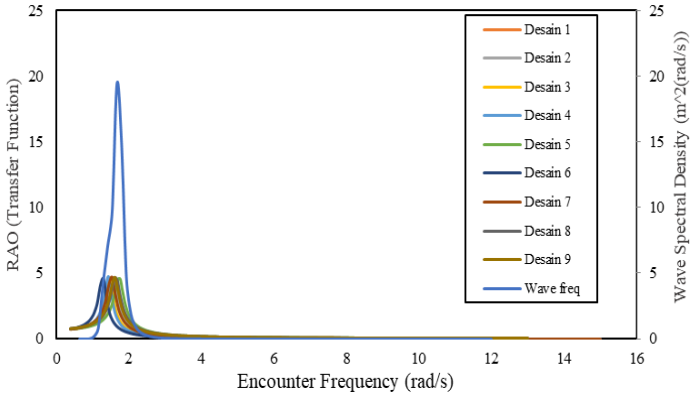

Fig. 24. RAO transfer function roll motion angle of incident wave 135°

Fig. 24 shows a roll motion graph of the effect of a wave force with an angle of incidence of 135° and a speed of 30 knots. The chart shows that the roll motion wave frequency is much higher than the design RAO. The RAO peaks of each design are close together and have almost the same height. Design 3 has the smallest peak value with an encounter frequency of 1.33 rad/s and a wave spectral density of 4.56 m²s/rad. The highest peak is in Design 9, with an encounter frequency of 1.62 rad/s and a wave spectral density of 4.71 m²s/rad. The height of the wave frequency is the encounter frequency that reaches 1.43 rad/s, and the wave spectral density of 19.46 m²s/rad. At the angle of incidence of 135°, it is known that the angle of incidence is quite influential on the ship's roll with the peak wave frequency and design RAO, which is quite high below the angle of 90°.

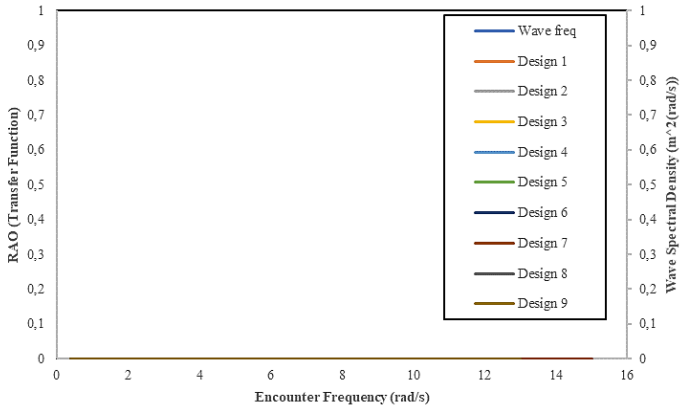

Fig. 25. RAO transfer function roll motion angle of incident wave 180°

Fig. 25 shows a roll motion graph of the effect of a wave force with an angle of incidence of 180° and a speed of 30 knots. The graph shows that wave frequency and design RAO value is 0. The simulation result shows that the wave's angle of incidence is 180° and does not affect the ship's roll.

The results of the roll analysis on seakeeping show the level of the ship's oscillation against the waves from all three angles. At 90°, the peak wave frequency at the frequency counter is 1.4 rad/s, and the ROA Roll peak value for the whole design is between 1.2 rad/s to 1.6 rad/s. At an angle of 135°, the wave frequency peaks when the counter frequency is 1.4 rad/s and the ROA Roll peak value for the whole design is between 1.2 rad/s to 1.6 rad/s. In contrast to heave and pitch, roll at a wave angle of 180° has an RAO Roll value of 0. So, it can be seen that the angle of incidence of a wave of 180 does not affect the ship's oscillation level. From the three angles of incidence, there is also no superposition between the RAO roll and the frequency counter. Indicates that the entire design is still in stable condition.

Fig. 23 shows that at an angle of 90° the design with the lowest response is Design 3 when the counter frequency is 1.3 rad/s. At an angle of 135°, the design that has the lowest response is Design 3, when the counter frequency is 1.3 rad/s. So that in this seakeeping roll motion, Design 3 has the stability of the ship's rocking motion to roll over better. The difference between the designs is not too far, and the whole is still in good stable condition.

4.4 Motion Sickness Incidence and Deck Wetness

Fast patrol boats at high speeds and big waves will certainly affect passenger comfort. The results of the simulation design Motion Sickness Incidence are presented in Fig. 26 and 27. Fig. 26 shows that passengers do not experience seasickness because the speed line does not intersect and exceeds the limit line. In comparison, Fig. 27 shows that at a speed of 30 knot, passengers can experience seasickness when the ship sails for 8 hours.

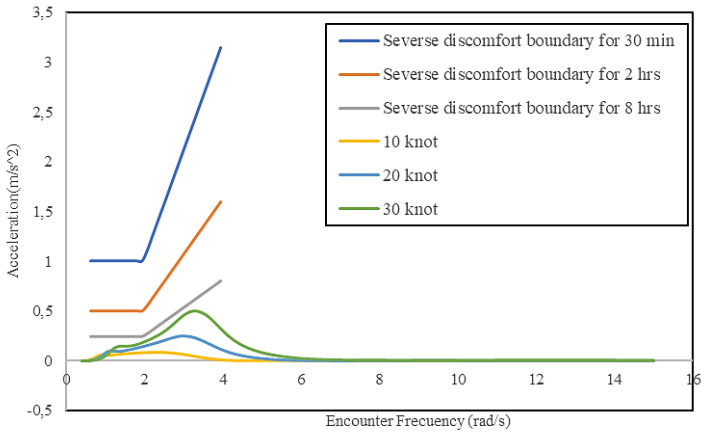

Fig. 26. Motion Sickness Incidence Design 7 angle of incidence of wave 180° and wave height of 0.5 m

Fig. 26 shows that the value of the seasickness level of passengers does not cross or intersect with the reverse discomfort boundary for 8 hours. At a speed of 30 knots, the graph has a peak acceleration value of 0.49 m/s² and an encounter frequency of 3.32 rad/s. The design that does not have a seasick line crossing the reverse discomfort boundary for 8 hours shows that the crew is more comfortable and does not experience seasickness during the 8-hour journey.

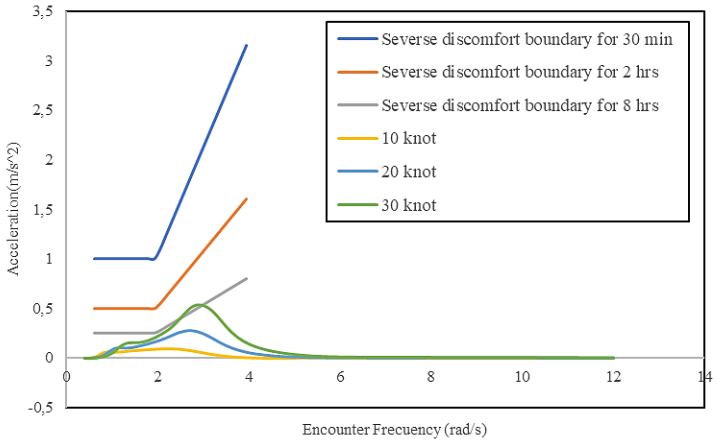

Fig. 27. Motion Sickness Incidence Design 1 angle of incidence of wave 180° and wave height of 0.5 m

From the MSI results, it is known that the overall design at a speed of 10 and 20 knot has a low value. Indicates that the ship is safe and the level of drunkenness for passengers is low. However, at a speed of 30 knot and a wave height of 0.5 m, some ships have a watering that begins to intersect and exceed the limit. It can be seen in Fig. 27 that the speed of 30 knot exceeds the safety value of the drunk limit for 8 hours. Design 1 peak at a speed of 30 knot achieves an acceleration of 5.3 m/s² with a counter frequency of 2.8 rad/s. Design 2, Design 3, Design 5, Design 8, and Design 9 at 30 knots also crossed the hangover limit at 8 hours of sailing, so the MSI Design 4, Design 6, and Design 7 simulations are safer designs for passenger safety because it has a lower chart of seasickness limit while sailing 8 hours. Extreme weather and high waves can make passengers seasick and cause wetness on the ship's deck. Wetness which can affect the stability of this ship, needs to be taken into account for better ship safety. The results of the deck wetness analysis on the nine ships are presented in Tables 11 to Table 13.

Table 11. Deck wetness value at an angle of incidence 90°

Speed (knot)	Design 1	Design 2	Design 3	Design 4	Design 5	Design 6	Design 7	Design 8	Design 9	Unit
10	1.891	4.432	1.403	1.966	2.725	2.416	1.277	1.929	2.044	MII/h
20	1.901	4.43	1.413	1.975	2.731	2.42	1.289	1.942	2.057	MII/h
30	1.909	4.431	1.421	1.983	2.736	2.427	1.3	1.951	2.065	MII/h

Table 11 shows the simulation of the deck wetness of nine ships at a wave angle of 90°. The deck wetness level at 10 knots was the highest in Design 2, with a value of 4.432 MII/h, and the lowest in Design 7, with a value of 1.277 MII/h. At a speed of 20 knots, the highest value is Design 2, with a value of 4.43 MII/h, and the smallest is Design 7, worth 1,289 MII/h. At a speed of 30 knots, the highest level of wetness is found in Design 2 with a value of 4.432 MII/h and the smallest at design 7 of 1.3 MII/h. The simulation results of the 90° angle of incidence show that Design 7 has a lower level of wetness.

Table 12. Deck wetness value at an angle of incidence 135°

Speed (knot)	Design 1	Design 2	Design 3	Design 4	Design 5	Design 6	Design 7	Design 8	Design 9	Unit
10	0.063	0.247	0.034	0.063	0.116	0.081	0.032	0.071	0.083	MII/h
20	0.096	0.254	0.061	0.12	0.139	0.109	0.054	0.099	0.127	MII/h
30	0.363	0.538	0.384	0.69	0.318	0.462	0.246	0.278	0.414	MII/h

Table 12 is the result of the simulation of the deck wetness of nine ships at a wave angle of 135°. The deck wetness level at a speed of 10 knots was highest in Design 2 with a value of 0.247 MII/h and the lowest in Design 7 with a value of 0.032 MII/h. At a speed of 20 knots, the highest value is Design 2, with a value of 0.254 MII/h and the smallest is Design 7, with a value of 0.054 MII/h. At a speed of 30 knots, the highest level of wetness is found in Design 2 with a value of 0.538 MII/h, and the smallest is in Design 7 with 0.246 MII/h. The simulation results of the 135° incident wave angle show that Design 7 also has a lower wetness level than other designs.

Table 13. Deck wetness value at an angle of incidence 180°.

Speed (knot)	Design 1	Design 2	Design 3	Design 4	Design 5	Design 6	Design 7	Design 8	Design 9	Unit
10	0	0	0	0	0	0	0	0	0	MII/h
20	0.003	0.001	0.004	0.015	0	0.002	0.002	0.001	0.005	MII/h
30	0.629	0.347	0.733	1.25	0.269	0.554	0.515	0.359	0.743	MII/h

Table 13 shows a simulation of the deck wetness of nine ships at a wave angle of 180°. The wettability of the nine designs is 0 at 10 knots, so it is known that at 10 knots, the deck cannot wet. At a speed of 20 knots, the highest value is Design 9, with a value of 0.005 MII/h and the smallest is Design 2 and Design 8, with a value of 0.001 MII/h. At a speed of 30 knots, the highest level of wetness is found in Design 4 with a value of 1.25 MII/h and the smallest in design 5 at 0.269 MII/h. The angle of incidence of the wave 180° indicates that the effect on the wetness of the deck is relatively small.

The deck wetness test is divided into three incident wave angles: 90°, 135°, and 180°. The probability of hourly deck wetness in all proposed designs is not bad. However, for the smallest hourly deck wetness value at 90° and 135° wave angles, namely Design 1, Design 3, and Design 7. But at 180° wave angle, the best results are Design 2, Design 5, and Design 8. This deck wetness Design 1, Design 3, and Design 7 are superior in deck wetness criteria at 90° and 135° wave angles. The 180° angle also has a pretty good hourly wettability value, though not the best of the other designs.

4.5 Floodable Length Curve

Floodable length simulation considers the prevention when the ship leaks, so it doesn't sink easily. The graph shows the maximum height of the compartment and the allowable flood length on the ship. The floodable length simulation results are shown in Fig. 28 and 29. Fig. 28 it results from floodable length where no compartment exceeds the flood limit. While Fig. 29 is the result of floodable length where there is a compartment that exceeds the flood limit.

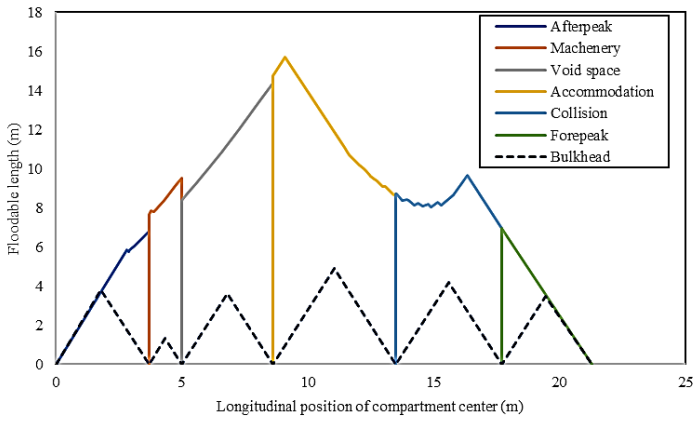

Fig. 28. Floodable length curve Design 7 bulkhead variations 1

Fig. 28 shows the results of the floodable length simulation in Design 7 with a bulkhead variation of 1. Design 7 with a bulkhead variation of 1 is one of the results which shows that no compartment triangle crosses the flood boundary line. Design 7 with a bulkhead variation of 1 is also a good result among the others because it has a relatively small average peak point. These results show that designs that do not have a compartment triangle crossing the boundary line have a higher and safer survival rate.

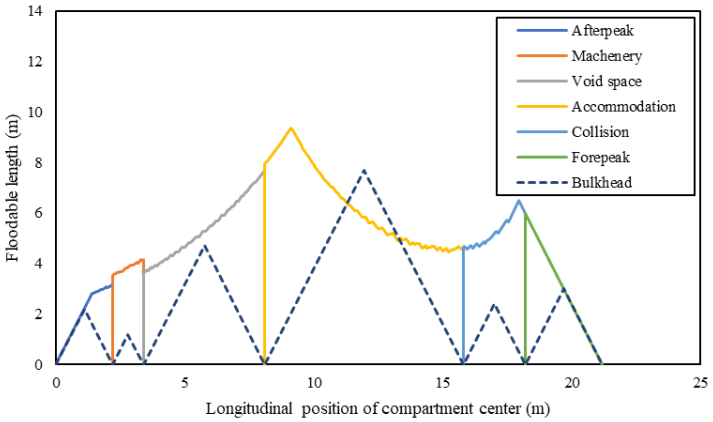

Fig. 29. Floodable length curve Design 2 bulkhead variations 3

Fig. 29 shows the simulation results of the flood length in Design 2 with a variety of bulkheads. Design 2 with a variation of bulkhead 3 is one of the results showing that compartments cross the flood boundary. These results indicate that when a ship leaks and water fill the compartment, the ship is difficult to survive and less safe. In the design, there are 2 dangerous rooms, namely the accommodation space where the room shows a high triangle line and exceeds the flood limit.

The results of floodable length at each compartment height and flood limit are influenced by the distance between the bulkhead and hull. Fig. 28 is one of the compatible results where each bulkhead does not exceed the allowable flood limit. The difference in the bulkhead distance in each variation shows how influential it is on the compartment. Fig. 29 shows room accommodation exceeds the allowable flood limit because the distance is quite far. Cases like this require further study or dividing the compartment into two in order to obtain the lower triangle. The bulkhead 1 and 2 bulkhead variations only found 1 design that did not meet the criteria, namely Design 2. In the Bulkhead 3 variation, three designs did not meet the criteria: Design 3, Design 5, and Design 8. So, in this floodable length simulation, Design 1, Design 4, Design 6, and Design 7 are safe and the best designs for flooding because from several variations, there is no compartment that exceeds the flood limit.

5 CONCLUSIONS

From the research conducted, various results were obtained using several ship testing criteria. However, there is no single design that shows the best results in all criteria. This shows that an aspect influences each criterion. So, from this, it is necessary to recapitulate to find out a better design among the proposed designs. Designs will be sorted from the best to each simulation performed. The recapitulation of design values in each simulation is shown in Table 14.

From the research conducted, various results were obtained from several ship testing criteria. However, the simulation results do not show the design with the best results across all criteria. Therefore, it is necessary to recapitulate to find a better design among the proposed designs. All designs will be ranked for each simulation performed from I which the best to IX which is the worst. Designs with a small number of values can be seen as designs with the best average test results because each design simulation has a reasonably good value, even the best from other designs. A recapitulation of the design values for each simulation is shown in Table 14.

Table 14. Recapitulation of design values in each simulation

Type of Simulation	Design								
	1	2	3	4	5	6	7	8	9
Resistance	VII	IX	V	I	VIII	II	III	VI	IV
Large Angle Stability	VIII	IX	IV	I	VI	III	II	V	VII
Seakeeping Heave Motion	VIII	IX	VI	IV	II	V	I	III	VII
Seakeeping Pitch Motion	VIII	IX	IV	III	VI	II	I	V	VII
Seakeeping Roll Motion	VII	IV	I	VIII	III	II	VI	V	IX
Motion Sickness Incidence	VI	V	VII	IX	I	IV	II	III	VIII
Deck wetness	III	VIII	II	VI	V	VII	I	IV	IX
Floodable length	IV	V	VII	III	VIII	II	I	VI	IX
Total Point	51	58	36	35	39	27	17	37	60

This study presents a simulation investigation of the hull model to obtain the most optimal design for the design of the Fast Patrol boat. The results of the simulation data recapitulation show that Design 7 has the best value among other designs. The results of the sequence of each of the best Design 7 simulations on Seakeeping Heave Motion, Seakeeping Pitch Motion, Deck wetness, and Floodable length. In other simulations, Design 7 also has a fairly good value and is not far adrift among other designs in the simulation of Resistance, Large Angle Stability, Seakeeping Roll Motion, and Motion Sickness Incidence. In addition, the design that is not good is found in design 9, where each simulation has the largest average value so that the design recommendations for Fast Patrol boats are obtained among the nine proposed designs, namely Design 7. In resistance result, Design 7 is the third best after Design 4 and Design 6, but at low speed, Design 7 is better than Design 6. Design 7 on resistance simulation results has a maximum value of 84645.71 N and power of 2870665.36 W. In the Large Angle Stability simulation, Design 7 is second after Design 4. Design 7 has a good level of stability by meeting all stability criteria specified with a maximum GZ of 0.984 m and an angle of maximum GZ of 52.7°.

The design 7 seakeeping simulation has the best value on heave motion and pitch motion but on the fourth best roll motion. The peak wave frequency of the maximum speed of Heave motion is found in Design 7 at a wave angle of 90° when the encounter frequency is 2.6 rad/s. The angle of incidence of the wave is 135° when the encounter frequency is 3.2 rad/s, and the angle of incidence of the wave is 180° when the encounter frequency is 3.2 rad/s. In

Pitch Motion Design 7 when the angle of incidence of the wave is 90°, and the encounter frequency is 1.7 rad/s. The angle of incidence of the wave is 135° when the encounter frequency is 3.2 rad/s, and the angle of incidence of the wave is 180° when the encounter frequency is 3.2 rad/s. The simulation results of Seakeeping Roll Motion, the peak value of each design, are not too far apart. Design 7 in the fourth order with a peak wave frequency angle of 90° waves when the encounter frequency is 1.5 rad/s. At the angle of incidence of wave 135°, when the encounter frequency is 1.5 rad/s.

Simulation Motion Sickness Incidence (MSI) Design 7 is the second best after Design 5, which has a slight difference in peak values at maximum speed. MSI Design 7 does not indicate that passengers can get seasick while sailing for 8 hours with a maximum speed and a wave height of 0.5 m. Design 7 has the highest peak value of 0.96 m/s² at a speed of 30 knot with a wave angle of 180° and waves of 0.5 m.

From the deck wetness value in the best deck wetness Design 7 simulation with a maximum speed value of 1.3 MII/h at the angle of incidence of wave 90°. At the angle of incidence, wave 135° has a value of 0.246 MII/h and a value of 0.515 MII/h at the angle of incidence wave 180°. Simulation of leakage prevention, namely floodable length Design 7 also has the best results with no bulkhead exceeding the allowable flood limit. Design 7 has an average triangular bulkhead height that is quite far from the flood limit of the three bulkhead variations used. So that the simulation of floodable length Design 7 is feasible and prevents ship flooding.

Design 7 is a design with reference to the Grandweld Shipyard Delivers 21M Discovery Class Vessel Fujairah Pilot. This design is superior to other proposed designs and can be recommended for the realization stage. It meets the set standards and, on average, has the best value in each simulation. Design 7 has good stability against the influence of external forces, minimal to the wetness of the deck when there is a big wave. In the leak prevention simulation, Design 7 has a satisfactory result with no triangles that cross the flood boundary of the three proposed bulkheads. It has a small triangular mean value and a large flood limit, making Design 7 better than the others. In terms of developing Design 7, further and specific developments are needed to make it more optimal. Design 7 in terms of Resistance, Large Angle Stability, Roll Motion Seakeeping, and Motion Sickness Incidence. Even though it has a good score and meets the requirements, it can be more improved achieve better characteristics and more satisfying simulation results.

6 ACKNOWLEDGMENTS

This work was supported by the RKAT PTNBH Universitas Sebelas Maret–Year 2023, under Research Scheme of “Penelitian Unggulan Terapan” (PUT-UNS), with Research Grant/Contract No. 228/UN27.22/PT.01.03/2023. The support is gratefully acknowledged by the authors.

7 REFERENCES

[1] Rumaji, R., Adiliya, A. (2019). Port Maritime Connectivity in South-East Indonesia: A New Strategic Positioning for Transhipment Port of Tenau Kupang. *The Asian Journal of Shipping and Logistics*, vol. 35, no. 4, 172–180, DOI: 10.1016/j.ajsl.2019.12.004.

[2] Rizal, N., History, P., Model, S., Perpendiculars, L.B. (2018). Resistance Test of Fast Patrol Ships in the Islands of Indonesia. *Journal of Ocean, Mechanical and Aerospace-Science and Engineering*, vol. 58, no. 1, 6–11.

[3] Dipua, A., Harahap, N., Puspitawati, D., Aminuddin, F., Prakoso, L.Y. (2021). Sea Defense Strategy the Indonesian Navy in Dealing with the South China Sea Conflict. *Italienisch*, vol. 11, no. 2, 120–126.

[4] Sutanto, R., Suseto, B., Warka, I.W., Sianturi, D., Rudiawan, B., Archipelago, I. (2021). Marine Defense Strategy In Facing the Threat of Transnational Crime In the Indonesian Archipelago Sea Lane I. *Review of International Geographical Education Online*, vol. 11, no. 10, 2318-2327.

[5] Risahdi, M., Jaddawi, M., Achmad, M., Henny, A., Prakoso, L. Y., Martani, W. R. (2020). Ambiguous policy on securing the vital objects of the Indonesian armed forces in East Java. *Public Policy and Administration Research*, vol. 10, no. 1, 52-56, DOI: 10.7176/ppar/10-1-08.

[6] Lajeunesse, A. (2021). Canada’s Arctic Offshore and Patrol Ships (AOPS): Their history and purpose. *Marine Policy*, vol. 124, 104323, DOI: 10.1016/j.marpol.2020.104323.

[7] Santos, F. M.; Temarel, P., Soares, C. G. (2009). Modal analysis of a fast patrol boat made of composite material. *Ocean engineering*, vol. 36, no.2, 179-192, DOI: 10.1016/j.oceaneng.2008.09.013.

[8] Prabowo, A. R., Febrianto, R. A., Tuswan, T., Tjahjana, D. D. D. P. (2022). Performance evaluation on the designed v-shaped monohull ship models. *Journal of Applied Engineering Science*, vol. 20, no. 2, 609-623, DOI: 10.5937/jaes0-29354.

[9] Ashkezari, A. Z., Moradi, M. (2021). Three-dimensional simulation and evaluation of the hydrodynamic effects of stern wedges on the performance and stability of high-speed planing monohull craft. *Applied Ocean Research*, vol. 110, 102585, DOI: 10.1016/j.apor.2021.102585.

[10] Rupenen, P. (2021). *Principles of Ship Buoyancy and Stability*. Aalto University Publication Series Science and Technology: Helsinki, Finland.

[11] Zhu, H., Hu, C. (2021). A unified seakeeping and maneuvering analysis of multiple linked towing system with triangular Bodies. *Ocean Engineering*, vol. 222, 108577, DOI: 10.1016/j.oceaneng.2021.108577.

[12] Luhulima, R. B., Setyawan, D., Utama, I. K. A. P., Utama, A. P. (2014). Selecting monohull, catamaran and trimaran as suitable passenger vessels based on stability and seakeeping criteria. In the International Ship Stability Workshop (ISSW): Kuala Lumpur, Malaysia.

[13] Hamoudi, B. (1995). *Dynamic response of hull due to bottom slamming and deck wetness*. ProQuest LLC: University of Glasgow: Glasgow, United Kingdom.

[14] Montewka, J., Manderbacka, T., Ruponen, P., Tompuri, M., Gil, M., Hirdaris, S. (2022). Accident susceptibility index for a passenger ship-a framework and case study. *Reliability Engineering & System Safety*, vol. 218, 108145, DOI: 10.1016/j.ress.2021.108145.

[15] Biran, A., López-Pulido, R. (2014). Flooding and Damage Condition. Ship Hydrostatics and Stability. Elsevier Ltd: Amsterdam, Netherlands, p. 259–290, DOI: 10.1016/b978-0-08-098287-8.00011-6.

[16] Davis, L. D.; Soreng, A. (2009). Twin Drive Gas Turbines in Single Proplusion Package for Norwegian Fast Patrol Boat. *In Turbo Expo: Power for Land, Sea, and Air*, vol. 48852, p. 949-957, DOI: 10.1115/GT2009-59222

[17] Febrianto, R. A., Prabowo, A. R., Baek, S. J., Adiputra, R. (2021). Analysis of Monohull Design Characteristics as Supporting Vessel for the COVID-19 Medical Treatment and Logistic. Transportation Research Procedia, vol. 55, p. 699-706, DOI: 10.1016/j.trpro.2021.07.038.

[18] Uhls, D. B. (2002). *Does the Fast Patrol Boat Have a Future in the Navy*?. University of Mississippi: Mississippi, United States.

[19] Aksu, S., Cannon, S., Gardiner, C., Gudze, M. (2002). *Hull Material Selection for Replacement Patrol Boats-An Overview*. DSTO Aeronautical and Maritime Research Laboratory: Fisherman's Bend, Australia.

[20] Prabowo, A. R., Martono, E., Muttaqie, T., Tuswan, T., Bae, D. M. Effect of hull design variations on the resistance profile and wave pattern: a case study of the patrol boat vessel. *Journal of Engineering Science and Technology*, vol. 17, no. 1, 106-126.

[21] Gotman, A. S. (2002). Study of Michell's integral and influence of viscosity and ship hull form on wave resistance. *Oceanic Engineering International*, vol. 6, no. 2, 74-115.

[22] Brizzolara, S. (2004). Parametric optimization of SWAT-hull forms by a viscous-inviscid free surface method driven by a differential evolution algorithm. In Proceedings 25th Symposium on Naval Hydrodynamics: St. John's, Newfoundland and Labrador, vol. 5, p. 47-64.

[23] Utama, I. K. A. P. (1999). Investigation of the viscous resistance components of catamaran forms. Doctoral dissertation - University of Southampton: Southampton, United Kingdom.

[24] Lewis, E. V. (1998). *Principles of Naval Architecture (second revision).* The Society of Naval Architects and Marine Engineers: Jersey, United States.

[25] Sun, H., Faltinsen, O. M. (2010). Numerical study of planing vessels in waves. *Journal of Hydrodynamics*, vol. 22, no. 1, 451-458, DOI: 10.1016/S1001-6058(09)60238-9.

[26] Rott, N. (1990). Note on the history of the Reynolds number. *Annual review of fluid mechanics*, vol. 22, no. 1-12, DOI: 10.1146/annurev.fl.22.010190.000245.

[27] Wu, H., He, J., Liang, H., Noblesse, F. (2019). Influence of Froude number and submergence depth on wave patterns. *European Journal of Mechanics-B/Fluids*, vol. 75, 258-270, DOI: 10.1016/j.euromechflu.2018.10.018.

[28] Lawther, A., Griffin, M. J. (1998). Motion sickness and motion characteristics of vessels at sea. *Ergonomics*, vol. 31, no. 10, 1373-1394, DOI: 10.1080/00140138808966783.

[29] Khai, D. Q., Quynh, N. T. T., Chien, N. M. (2021). A Comparison Study on the Resistance Calculation of Planning Boat. *International Journal of Engineering Applied Sciences and Technology*, vol. 5, 23–26, DOI: 10.33564/ijeast.2021.v05i12.003.

[30] Tarafder, M. S., Saaki, A. R. (1980). Computation of resistance of high speed planing craft using Savitsky's theory. *AIP Conference Proceedings*, vol. 1980, 040006, DOI: 10.1063/1.5044316.

[31] Julianto, R. I., Prabowo, A. R., Muhayat, N., Putranto, T., Adiputra, R. (2021). Investigation of hull design to quantify resistance criteria using Holtrop's regression based method and Savitsky's mathematical model: a study case of fishing vessels. *Journal of Engineering Science and Technology*, vol. 16, no. 2, 1426-1443.

[32] Biran, A., López-Pulido, R. (2013). *Ship hydrostatics and stability*. Butterworth-Heinemann: Oxford, United Kingdom.

[33] Bačkalov, I., Bulian, G., Rosén, A., Shigunov, V., Themelis, N. (2016). Improvement of ship stability and safety in intact condition through operational measures: challenges and opportunities. *Ocean engineering*, vol. 120, 353-361, DOI: 10.1016/j.oceaneng.2016.02.011.

[34] Krata, P. (2013). The impact of sloshing liquids on ship stability for various dimensions of partly filled tanks. *TransNav-The International Journal on Marine Navigation and Safety of Sea Transportation*, vol. 7, 481-489, DOI: 10.12716/1001.07.04.02.

[35] Ruponen, P., Manderbacka, T., Lindroth, D. (2018). On the calculation of the righting lever curve for a damaged ship. *Ocean Engineering*, vol. 149, 313-324, DOI: 10.1016/j.oceaneng.2017.12.036.

[36] Masoudi, E. (2017). Second generation IMO intact stability vulnerability criteria and its application to ships navigating in Persian Gulf and Oman Sea. *International Journal of Maritime Technology*, vol. 7, 39-48, DOI: 10.18869/acadpub.ijmt.7.39.

[37] Huang, L.; Deng, X., Bo, Y., Zhang, Y., Wang, P. (2022). Evolutionary optimization assisted delayed deep cycle reservoir modeling method with its application to ship heave motion prediction. *ISA transactions*, vol. 126, 638-648, DOI: 10.1016/j.isatra.2021.08.020.

[38] Ueng, S. K., Lin, D., Liu, C. H. (2008). A ship motion simulation system. *Virtual realit*y, vol. 12, no. 1, 65-76, DOI: 10.1007/s10055-008-0088-8.

[39] Yin, J. C., Zou, Z. J., Xu, F. (2013). On-line prediction of ship roll motion during maneuvering using sequential learning RBF neuralnetworks. *Ocean Engineering*, vol. 61, 139-147, DOI: 10.1016/j.oceaneng.2013.01.005.

[40] Aranda, J., De la Cruz, J. M., Diaz, J. M. (2005). Design of a multivariable robust controller to decrease the motion sickness incidence in fast ferries. *Control Engineering Practice*, vol. 13, no. 8, 985-999, DOI: 10.1016/j.conengprac.2004.11.003.

[41] Nguyen, V. M., Jeon, M. J., Yoon, H. K. (2016). Study on the optimal weather routing of a ship considering parametric rolling, slamming and deck wetness. Proceedings of PRADS2016, vol. 4.

[42] Biran, A., Pulido, R. L. (2014). *Flooding and Damage Condition, in Ship Hydrostatics and Stability (Second Edition)*. Butterworth-Heinemann: Oxford, United Kingdom.

[43] Kałkowska, E. (2017). Floodable length of a bulk carrier. *Zeszyty Naukowe Akademii Morskiej w Szczecinie*, vol. 51, no. 123, 71-77.

[44] Kuznecovs, A., Schreuder, M., Ringsberg, J. W. (2021). Methodology for the simulation of a ship's damage stability and ultimate strength conditions following a collision. *Marine Structures*, vol. 79, 103087, DOI: 10.1016/j.marstruc.2021.103027.

[45] Nam-Kyun, I. M., Hun, C. (2021). A quantitative methodology for evaluating the ship stability using the index for marine ship intact stability assessment model. *International Journal of Naval Architecture and Ocean Engineering*, vol. 13, 246-259, DOI: 10.1016/j.ijnaoe.2021.01.005.

[46] Woo, D., Choe, H., Im, N. K. (2021). Analysis of the Relationship between GM and IMO Intact Stability Parameters to Propose Simple Evaluation Methodology. *Journal of Marine Science and Engineering*, vol. 9, no. 7, 735, DOI: 10.3390/jmse9070735.

[47] Yao, C., Huang, J., Sun, X., Yu, J., Feng, D. (2021). Numerical investigation of side-wall effects on the seakeeping performance of a ship advancing in waves. *Ocean Engineering*, vol. 239, 109797, DOI: 10.1016/j.oceaneng.2021.109797.

[48] Wang, S. M., Ma, S., Duan, W. Y. (2018). Seakeeping optimization of trimaran outrigger layout based on NSGA-II. *Applied Ocean Research*, vol. 78, 110-122, DOI: 10.1016/j.apor.2018.06.010.

[49] Scamardella, A.; Piscopo, V. (2014). Passenger ship seakeeping optimization by the Overall Motion Sickness Incidence. *Ocean Engineering*, vol. 76, 86-97, DOI: 10.1016/j.oceaneng.2013.12.005.

[50] Dhavalikar, S., Dabbi, P. N., Poojari, D., Joga, R., Awasare, S. (2018). Development of empirical formulation for bow flare slamming and deck wetness for displacement vessels. *Journal of Marine Science and Application,* vol. 17, no. 3, 414-431, DOI: 10.1007/s11804-018-0045-1.

[51] Pennanen, P., Ruponen, P., Nordström, J., Goerlandt, F. (2016). Application of vessel TRIAGE for a damaged passenger ship. In the International Ship Stability Workshop (ISSW): Stockholm, p. 141-146.

[52] Julianto, R. I., Muttaqie, T., Adiputra, R., Hadi, S., Hidajat, R. L. L. G., Prabowo, A. R. (2020). Hydrodynamic and Structural Investigations of Catamaran Design. *Procedia Structural Integrity*, vol. 27, 93-100, DOI: 10.1016/j.prostr.2020.07.013.

[53] Medina, J. R., Molines, J., Escrivá, J. A. G.; Aguilar, J. (2020). Bunker consumption of containerships considering sailing speed and wind conditions. *Transportation Research Part D: Transport and Environment*, vol. 87, 102494, DOI: 10.1016/j.trd.2020.102494.

[54] Yusvika, M., Prabowo, A. R., Baek, S. J., Tjahjana, D. D. D. P. (2020). Achievements in Observation and Prediction of Cavitation: Effect and Damage on the Ship Propellers. *Procedia Structural Integrity*, vol. 27, 109-116, DOI: 10.1016/j.prostr.2020.07.015.

[55] Nyanya, M. N., Vu, H. B., Schönborn, A., Ölçer, A. (2021). Wind and solar assisted ship propulsion optimisation and its application to a bulk carrier. *Sustainable Energy Technologies and Assessments*, vol. 47, 101397, DOI: 10.1016/j.seta.2021.101397.

[56] Yusvika, M., Fajri, A., Tuswan, T., Prabowo, A. R., Hadi, S., Yaningsih, I., Muttaqie, T., Laksono, F. B. (2022). Numerical prediction of cavitation phenomena on marine vessel: Effect of the water environment profile on the propulsion performance. *Open Engineering*, vol. 12, no. 1, 293-312, DOI: 10.1515/eng-2022-0034.

[57] Rahmaji, T., Prabowo, A. R., Tuswan, T., Muttaqie, T., Muhayat, N., Baek, S. J. (2022). Design of Fast Patrol Boat for Improving Resistance, Stability, and Seakeeping Performance. *Designs*, vol. 6, 105, DOI: 10.3390/designs6060105.

Paper submitted: 17.10.2022.

Paper accepted: 17.04.2023.